THE EFFECTS OF NANOPARTICLE AUGMENTATION OF NITRATE THERMAL STORAGE MATERIALS FOR USE IN CONCENTRATING SOLAR POWER APPLICATIONS

A Thesis

by

MATTHEW ROBERT BETTS

Submitted to the Office of Graduate Studies of
Texas A&M University
in partial fulfillment of the requirements for the degree of

MASTER OF SCIENCE

May 2011

Major Subject: Mechanical Engineering

The Effects of Nanoparticle Augmentation of Nitrate Thermal Storage Materials for Use in Concentrating Solar Power Applications

THE EFFECTS OF NANOPARTICLE AUGMENTATION OF NITRATE THERMAL STORAGE MATERIALS FOR USE IN CONCENTRATING SOLAR POWER APPLICATIONS

A Thesis

by

MATTHEW ROBERT BETTS

Submitted to the Office of Graduate Studies of
Texas A&M University
in partial fulfillment of the requirements for the degree of

MASTER OF SCIENCE

Approved by:

Co-Chairs of Committee,	Thomas Lalk
	Michael Schuller
Committee Member,	Sy-Bor Wen
Head of Department,	Dennis O'Neal

May 2011

Major Subject: Mechanical Engineering

ABSTRACT

The Effects of Nanoparticle Augmentation of Nitrate Thermal Storage Materials for Use in Concentrating Solar Power Applications. (May 2011)

Matthew Robert Betts, B.S., Georgia Institute of Technology

Co-Chairs of Advisory Committee: Dr. Thomas Lalk
Dr. Michael Schuller

The Department of Energy funded a project to determine if the specific heat of thermal energy storage materials could be improved by adding nanoparticles. The standard thermal energy storage materials are molten salts. The chosen molten salt was a sodium nitrate and potassium nitrate eutectic, commercially called Hitec Solar Salt. Two nanoparticle types were chosen, alumina and silica. The nanoparticle composite materials were fabricated by mixing the components in an aqueous solution, mixing that solution for a set amount of time using a sonic mixer, then removing the water from the aqueous solution, leaving the composite molten salt behind as a fine white powder.

The thermal properties of the composite and plain material were measured using two techniques: American Society for Testing and Materials (ASTM) 1269E and Modulating Differential Scanning Calorimetry (MDSC). These two techniques measured the specific heat and the heat of fusion of the plain and composite materials.

The results of all the ASTM and MDSC measurements suggest that the addition of the nanoparticles using the given manufacturing technique increased the specific heat of the molten salt by approximately 20%, with both measurement techniques showing approximately the same level of increase. The silica and the alumina improved the specific heat by nearly the

same amount over the base material. The heat of fusion did not seem to be significantly altered compared to the observed heat of fusion value of the unmodified material.

It was also observed that the nitrate and silica composite material's specific heat decreased if the material was raised to a temperature above 400C. The specific heat was observed to decrease over time, even when the temperature was well below 400C. It is unknown why this occurred. The nitrate plus alumina composite and the plain nitrate were stable to a temperature of 450 C for the test duration.

DEDICATION

For my parents: I told you I was working down here.

For Saxony: No more sleeping in the lab.

ACKNOWLEDGEMENTS

I would like to thank my committee members for putting up with my many questions and insane schedule. Thanks also go to the coffee ladies in Blocker, as I never would have made it without them. I would also like to thank Dr. Reza Langari and Dr. Brian Rasmussen for letting me TA for them so I could get my bearings. My girlfriend, Saxony Scott, deserves a rack of medals for putting up with my work schedule. I appreciate my folks trusting me enough to take care of this thesis and deal with my own problems. Lastly, I'd like to thank Dr. Frank Little and Dr. Cable Kurwitz for giving me that little nudge when I was about to throw my hands up over the whole thing. I would like to acknowledge the help of Mr. Donghyun Shin for providing training on the synthesis protocols for carbonate salt based nanocomposites using the evaporation technique.

TABLE OF CONTENTS

Page

Page

LIST OF FIGURES

Page

Page

Page

LIST OF TABLES

Page

1. INTRODUCTION

As technology has marched inexorably forward, methods of generating electricity have been crucial to the advancement of science and improving lives everywhere. The vast majority of the electricity generated in the world today is created using limited resources, such as fossil or nuclear fuels. Alternative energy sources, such as wind, solar, and hydroelectric are gaining acceptance due to difficulties associated with fossil fuels. One of the means of improving the economic competitiveness of solar power is through the use of a storage system, which levels power delivery in case of clouds and provides power even when the sun is below the horizon. In these systems, various storage materials are used to improve performance, including molten salts. In particular, interest has been directed at nitrate eutectics. Nanoparticles have been combined with the standard nitrate eutectic in an effort to improve the thermal characteristics of the molten salt for use in thermal energy storage systems.

Current thermal energy storage systems are based around grid power scales, so store large quantities (MWhrs) of energy. Therefore, the systems are generally large and contain a large volume of storage material. Increasing the specific heat of the nitrate eutectic will decrease the quantity of material required to store a given amount of energy in a given system, reducing the storage system cost and size. Reducing the cost means thermal energy storage systems could be implemented in more locations, improving the viability of commercial concentrating solar power.

This thesis follows the style of *International Journal of Energy Research*.

Using additives to alter the properties of a mixture is nothing new. The many varieties of steel are a testament to that. The largest difference between the older mixtures and nanomaterials is the size of individual pieces of the additive. For currently unknown reasons, nanoparticles seem to have a much larger effect on thermal properties than the same material in standard form at certain low mixture mass percentages. Therefore, adding nanoparticles allows for the possibility of emulating or exceeding the properties of mixtures that use much more expensive materials. More importantly, the reduced quantity of nanoparticles relative to the bulk material required reduces the cost to get the improved performance.

Therefore, the primary objective of this investigation is to determine if the addition of ceramic nanoparticles alters the specific heat of the nitrate eutectic, and if so, to what degree. The secondary objective is to quantify the change, if any, of the heat of fusion of the nitrate eutectic. The tertiary objective is to determine if the nanoparticle nitrate composite is stable over time in the standard concentrating solar power storage temperature range. The final objective is to determine if the specific heat results from the first objective are observed using multiple measurement techniques.

2. BACKGROUND

The Department of Energy funded this experiment based on a proposal by Dr. Michael Schuller. The proposal was based on investigating the effects of adding nanoparticles to molten salts for use in thermal energy storage systems combined with concentrating solar power plants. Based on the proposal deliverables and input from the Department of Energy, a specific storage material was chosen and the testing temperature range was set. Therefore, to provide context for this experiment, several key systems used in concentrating solar power are explained below, including the most common collection systems and the thermal energy storage systems that can incorporate the composite nitrate material. The chosen storage material, a nitrate eutectic, is also examined in more detail.

2.1 Solar Power Concepts

Concentrating Solar Power (CSP) is an extremely old concept, with evidence showing it was an established method of heating as far back as the ancient Greeks, as shown by Archimedes's heat ray purportedly used in the siege of Syracuse. The conversion of steam into movement is almost as old, as shown by drawings from Heron of Alexandria and his steam engine. It is therefore a very clearly understood series of systems, and uses other well-established sub-systems to generate electricity from motive force. In that sense, CSP is a simple system, based on old and understood operating principles for the components and systems. Due to CSP's simpler operating principles and simpler components, a functional CSP plant can be set up almost anywhere there is sufficient direct sunlight, and can be maintained almost

indefinitely with a minimum of technical experience. Therefore, from a grid-level power generation perspective, CSP is applicable all over the world.

2.2 Expanded CSP Concept

The primary goal of any CSP plant is to focus the sun's radiation onto a receiver in order to heat it, then use the thermal energy input to the receiver to generate electricity. There are two main CSP concepts currently in use: a power tower and a parabolic trough system. There are several of these installations all over the world, with the newest being in Spain, and the oldest being in the Unites States. There was significant research done on and for these facilities during the 1970s and 1980s, but it is only lately that the CSP concept has seen a revival. Much of the drive for this revival stems from increasing pressure from ecological groups and the rising cost of standard fossil fuels. The two primary CSP systems, explained in greater detail later, can be easily differentiated by their focusing area. Power tower systems use a point focus area, meaning the radiation from the sun is focused on a single point or very small area. In comparison, a trough system focuses the sun's radiation on a line. Both approaches have their advantages and disadvantages, which will be expanded on later in this section.

2.2.1 Power Tower

Currently the most publicly seen type of CSP, a power tower is much like it sounds. A schematic view can be seen in Figure 1. A tall tower is placed in the center of a circular field of reflecting mirrors called heliostats, with a receiver placed at or near the top of the tower, where the radiation is focused. In current systems, the power loop fluid (usually water) is

cycled through the area until it is converted into superheated steam, at which point it is fed into the steam turbine of the plant's Rankine cycle for electric power conversion. An alternative to using water is to use a different fluid for the electricity generation loop and the transfer of thermal energy from the receiver to the electricity generation loop, usually called Heat Transfer Fluid (HTF). The power tower CSP system has received significant public exposure via commercial media, and has been seen in movies and video games. The exposure and public awareness of the system has made it more "reputable" than other CSP systems, despite the advantages and disadvantages of other types of CSP.

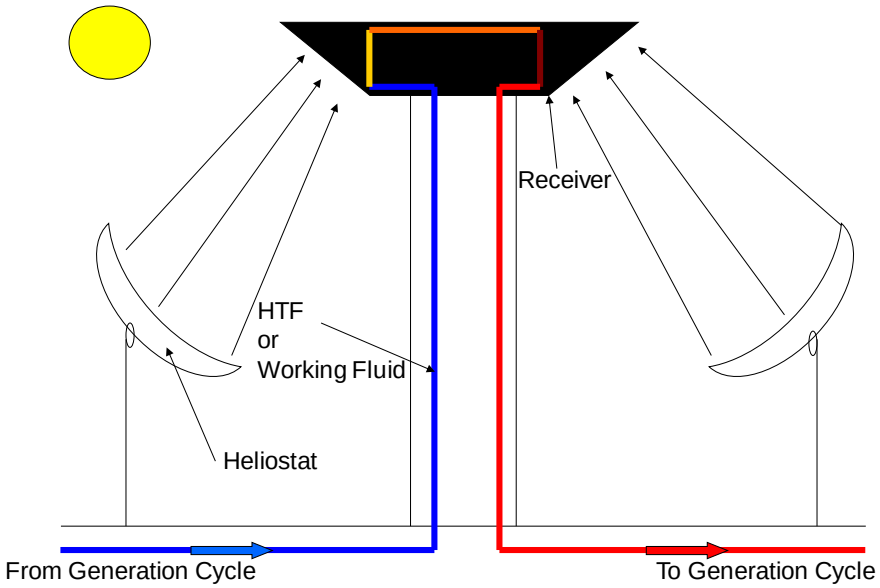

Figure 1: Schematic view of a power tower CSP system, showing the primary components. The sun's radiation is reflected and focused onto the receiver, which has the HTF or working fluid running through it. As more of the sun's radiation is focused onto the receiver, it becomes hot, raising the temperature of the working fluid as well. The hot working fluid is then run through an electricity generation cycle to complete the electricity conversion process from sunlight to electricity.

General problems with the power tower concept are the same as any solar power plant, namely a limited power generation window and weather limitations. Power tower

installations also require a considerable amount of land and have significant pumping power requirement, as the working fluid must be pumped up several hundred feet in order to flow through the receiver. The receiver must be elevated to receive thermal energy from more than one row of heliostats. Also, the large heliostat field requires constant cleaning, as any contamination on the heliostats will significantly reduce the effectiveness of the reflection. Advantages of the power tower over other solar installations are generally related to the power tower itself. The general restriction of the working fluid to a single building helps reduce the amount of piping losses and potential leak sites. Power towers are also able to attain higher output temperatures than other CSP types, up to 600C, significantly increasing the power output per acre of land required over a trough system. The extreme localization of the working fluid also makes incorporation of a thermal storage system far easier compared to a trough system, as the HTF is only in the actual tower or close by, rather than throughout the entire heliostat field.

2.2.2 Trough Systems

Trough systems are large fields of horizontal parabolic dishes that focus the sun's radiation onto a pipe suspended a short distance above the trough. A schematic view can be seen in Figure 2. Rather than redirecting the energy to a central location located at least several hundred feet away, the dishes focus energy onto a pipe suspended slightly above the trough, which is filled with the working fluid or HTF. In this way, the facility can be any shape or size without compromising effectiveness. The hot working fluid is then pumped to a standard Rankine cycle to generate electricity. Advantages of the trough system include increased

modularity and ease of scaling, as new troughs can be added just by expanding the pipe network. This allows trough CSP plants to expand as needed, whereas a power tower system can only be expanded so far before an additional tower is required, which would effectively be a new plant. Also, particulates in the atmosphere pose less of a problem for a trough system, as the optical transmission distance is much shorter. The overall system is also much more forgiving of site issues, such as changes in elevation or existing structures. In this manner, the trough system can be incorporated into cities, roads, and other existing infrastructure with less disruption than a power tower, which requires very flat and completely empty land.

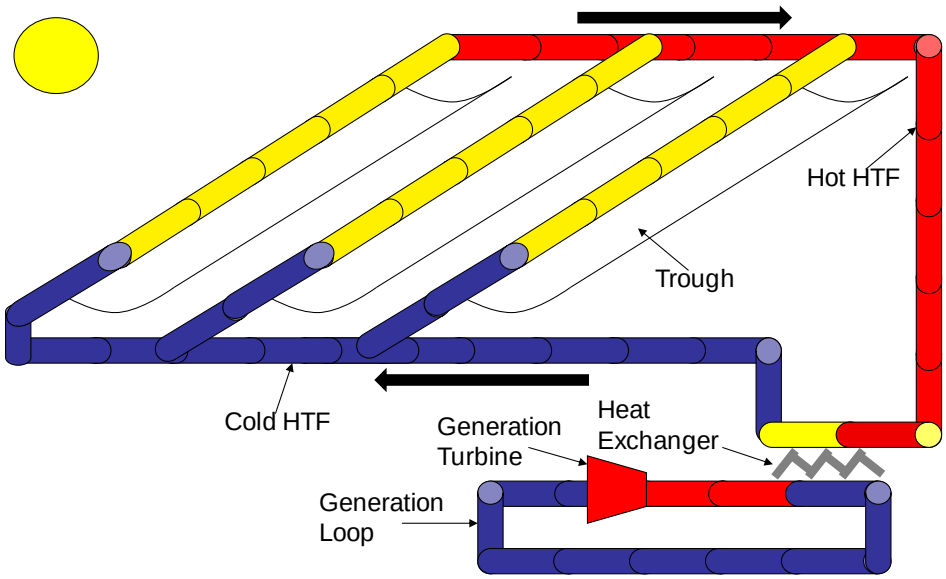

Figure 2: Schematic view of a parabolic trough CSP system, showing the troughs, HTF flow loop, and the generation loop.

Disadvantages of parabolic trough systems are primarily linked to the focusing abilities of the trough. Parabolic trough systems generate lower maximum temperatures due to the lower energy density possible on the surface of the transfer pipe. This is because the energy

reflected by the trough is spread out over the length of the trough, whereas a power tower has the energy from hundreds of heliostats focused on a small area, providing drastically increased energy density compared to the trough systems. Trough systems are also more susceptible to leaks of the transfer fluid, both thermal and physical. The heat loss through a trough system's non-trough zones can be ameliorated somewhat by extensive insulation, but the hot fluid still has a significant distance to go until it transfers its energy into the power cycle loop. The trough system requires many pipe segments outdoors and exposed to the elements. The pipe sections also undergo many thermal cycles, as they cool when the sun is not radiating into the trough. The combination of thermal cycles and external wear frequently makes trough systems require additional maintenance to prevent HTF leaks.

One of the key problems with all CSP systems is the reliance on the sun. The sun is not a constant power source, and is often blocked by weather or by night. The established way to fix this problem is to use a thermal energy storage system.

2.3 Thermal Energy Storage Systems

One of the primary problems with all CSP systems is their output variability depending on the weather. Moreover, more than one factor of the weather determines the instantaneous energy delivery to the plant collectors. Since many weather factors change quickly, the resultant power output of the plant changes over the course of a day. Additionally, the plant will only generate electricity while the sun is out, so during the non-operational periods of the day, the plant makes no power and consumes power to maintain the systems at operational readiness. Lastly, unlike traditional fossil, hydroelectric, or fission plants, CSP plants cannot be

“throttled up” to provide more power during peak draw periods, as there is no way to get more energy from the plant than the sun provides. One way to ameliorate these problems is with an energy storage system. An energy storage system allows the operator to accept all the power possible (unless the system is fully charged) from the sun when demand is low, then shunt additional energy to the plant output when the sun alone is insufficient. An energy storage system also counters any short-term solar disruption, such as clouds, a sandstorm, or other weather effects so the plant can continue producing electricity.

Thermal Energy Storage systems, (TES) as the name implies, store energy by keeping something out of thermal equilibrium with the environment, then use the thermal potential as the energy storage mechanism. TES systems have the advantage of being applicable in most current electricity generation plants as a direct supplement in the existing electricity conversion systems, which are usually Rankine cycle turbines. This allows the TES system cost to be lower, as it uses existing energy conversion systems already used by the power plant, rather than using additional expensive hardware. Other non-electric energy storage systems may require additional electrical energy conversion hardware, such as a turbine in a hydroelectric dam. Even electric energy storage systems, such as capacitor banks or static VAR compensators frequently require additional electricity conditioning and control equipment, significantly increasing their cost.

TES systems match extremely well with the expected operation of a CSP plant for several reasons. TES systems and CSP plants both use thermal energy as the primary energy form, allowing for easy integration. TES systems are fully scalable, so a TES system could be designed to level the plant’s energy output over a full 24 hours, rather than just when the sun is up. Alternatively, if the electricity generation cycle components are sized to accept it, the TES

system could augment the collected energy going into the electricity generation loop, allowing the plant to output more electricity to meet demand. This ability would be useful during peak demand hours, which typically comprise only part of the sunny hours of the day. Lastly, certain TES systems can be upgraded at a later date to suit changes in the plant by changing the energy storage material, rather than replacing the entire system. Each TES system type has its own advantages and disadvantages, which will be expanded on next.

There are currently three main types of thermal storage systems: thermocline, two-tank, and brick systems. They all operate using similar principles, but the implementation of those principles differs. Figure 3 shows how such a system is typically integrated into a CSP system. The system shown in Figure 3 is a parallel system, in that the electricity generation loop can receive energy from either the solar energy collection system or the TES, or both at the same time. Other implementations of TES systems can be serial systems, meaning all the energy from the solar energy collection system first goes through the TES before reaching the electricity generation system. Each of the TES types store thermal energy in the form of sensible energy, which means the energy is stored in the elevated temperature of a material. Other systems not covered here use latent energy storage, meaning they store energy not in temperature, but in the phase of a material. As an example, consider a pot of water. The thermal energy stored in the water can be broken down into two parts: the sensible energy and the latent energy. If the water is heated to 90 C but not boiled, then the thermal energy is purely sensible, as all the thermal energy is stored in the temperature of the water. However, if the water is raised to a higher temperature, such as 150 C and allowed to boil, then the thermal energy is stored in both the temperature of the steam and in the energy required to turn the liquid water into steam, which is the latent energy.

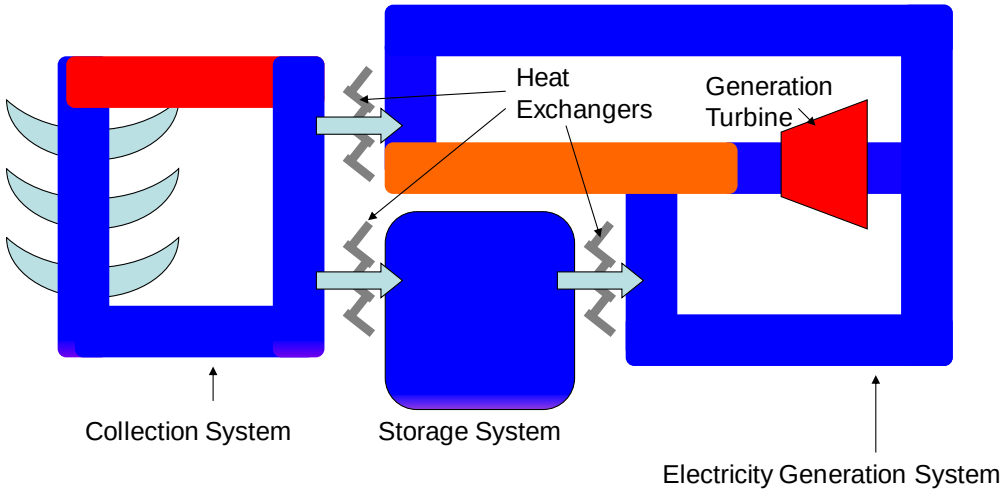

Figure 3: Complete CSP system with storage schematic view, showing the placement of a TES system in a power plant. The setup shown illustrates a parallel input system, as the generation system can receive energy from the TES system and the collection system simultaneously.

Each of the TES types, thermocline, two-tank, and brick, are discussed in greater detail in their own sections. Of the described systems, only the thermocline and two-tank can actually use the composite nitrate discussed in this investigation.

2.3.1 Thermoclines

A thermocline is basically a large thermal mass between the solar collector energy and the electricity generation system in a serial CSP system. In a parallel CSP system, the thermocline is linked with the solar collector energy and the electricity generation system, but the solar collector energy can also be transferred directly to the electricity generation system, bypassing the thermocline entirely. The simplest version of the system is comprised of four primary parts: a large tank, filler, a pair of heat exchangers, and the thermal energy storage material. The two heat exchangers link the thermal storage material to the solar collection

system and the electricity generation system. The tank is packed with the filler and the storage material. The hot HTF is pumped through the heat exchanger linking the collection system to the thermal energy storage material to heat the storage material and therefore charge the thermocline. The storage material then heats the filler by conduction and internal convection. The electricity generation system working fluid is run through the second heat exchanger linking the storage material to the electricity generation system to discharge the thermocline. The storage material chosen for this investigation is a nitrate eutectic called Hitec solar salt, which will be discussed in greater detail later. The filler is generally comprised of macro-sized solid material particles. The most common filler is processed sand. The combination of the storage material and the filler creates an aggregate thermal mass able to absorb considerable quantities of thermal energy per volume. A diagram showing a schematic view of a thermocline can be seen in Figure 4.

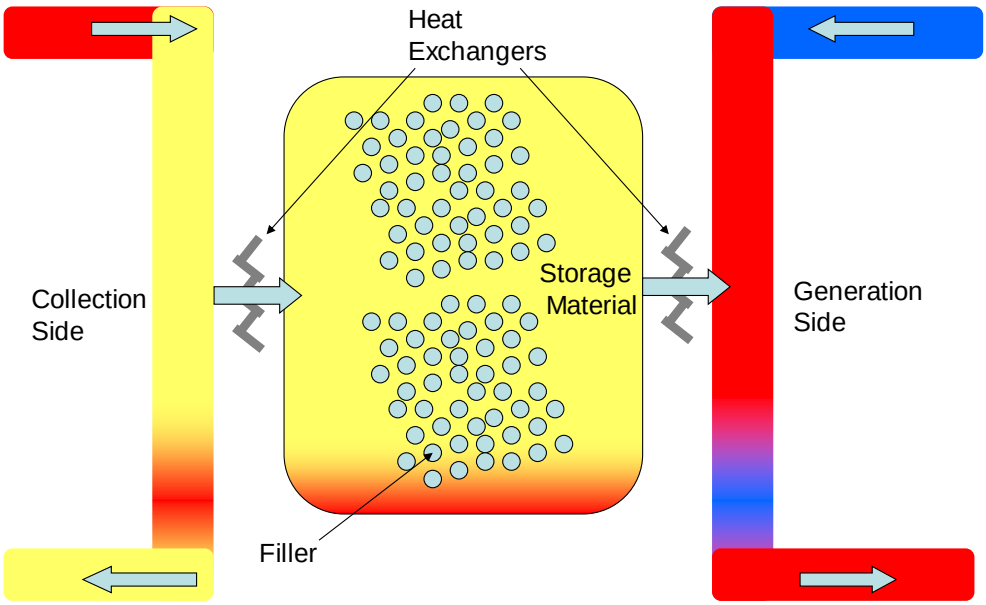

Figure 4: Thermocline schematic view, showing the components of a thermocline. The composite nitrate eutectic being investigated is a type of storage material as shown in the diagram.

The thermocline system's advantages are generally tied to its simplicity. The system itself has virtually no moving parts, and is unlikely to break, barring a volumetric expansion of the storage material. The system can hold a significant amount of energy depending on the tank size desired, and the system can be scaled with relative ease without causing significant system complications. On the downside, the thermocline system is generally quite large, and is therefore somewhat expensive due to the quantities of materials involved. The system typically has poor transient response due to its large size, which can limit the maximum thermal power input and output of the thermocline, although this can be mitigated by over-sizing the two heat exchangers.

There are several configurations of the basic thermocline design, depending on the materials used. As previously mentioned, the storage material and the heat transfer fluid (HTF) from the solar collector system can be the same material, but frequently are not. The two materials are usually different because they have different functions, and therefore different physical and thermal requirements. The HTF needs to have a high thermal conductivity, low viscosity, and a high specific heat in descending order of priority, meaning specific heat is the lowest listed priority. Specific heat is a relatively low priority because the energy carried by the transfer fluid can be modulated by varying the flow rate to compensate for a low specific heat. Similarly, the viscosity needs to be low to reduce the pumping energy required to circulate the HTF through the solar collection system. The storage material needs to have a high specific heat, a high thermal conductivity, and a low cost, once again in descending priority order. The storage material does not need to be pumped various places, so the specific heat plays the largest role in determining the potential energy storage capacity of a given volume, hence it is the largest priority. The thermal conductivity plays a significant role as it determines the heat

exchanger size needed to meet the power transfer capabilities of the TES system. The filler needs to have a high specific heat and be extremely cheap. The filler is used to cut the cost of the thermocline, as the filler is generally at least an order of magnitude cheaper than the storage material on a per-mass basis, while having a similar specific heat. The standard filler currently in use is sand, due to its extremely low cost and generally inert behavior.

A concern in a thermocline system is the requirement that the storage material must be in a liquid form to allow for circulation in the thermocline. Keeping the storage material in liquid form can be problematic, as the most common storage materials have melting temperatures of above 180 C. Therefore, many of the thermocline systems have auxiliary heaters to maintain the storage material in its liquid state. These heaters are frequently natural gas or electric units, so they require substantial external energy to function, increasing the cost of thermocline operation.

2.3.2 Two-Tank

The two tank system functions similarly to a thermocline in that the HTF is linked with a storage material, which is also linked with the electricity generation system, just as in the thermocline. However, in a two-tank system, the storage material is pumped between two tanks, one “hot”, one “cold”. Depending on the configuration of the system, two heat exchangers are used in the connection between the two tanks, which can be seen in Figure 5. In this setup, the connection between the tanks has a heat exchanger linked to the electricity generation cycle and a heat exchanger linking the storage material with the HTF. To charge a two-tank system, the cold storage material is pumped between the two tanks so it interfaces

with the HTF heat exchanger, raising the storage material's temperature. After the storage material has been through the HTF heat exchanger, it is pumped to the hot tank. Once all the storage material has been pumped from the cold tank, through the HTF heat exchanger, and into the hot tank, the system is fully charged, as all the storage material is at the maximum operating temperature of the system. The system is discharged by pumping the hot storage fluid from the hot tank, through the electricity generation cycle heat exchanger, then to the cold tank. The hot storage material transfers its thermal energy to the electricity generation cycle through the electricity generation cycle heat exchanger, and therefore decreases in temperature to the cold state. Once all the cold storage material has been pumped back into the cold tank after passing through the electricity generation cycle heat exchanger, the system is fully discharged, as all the storage material is cold.

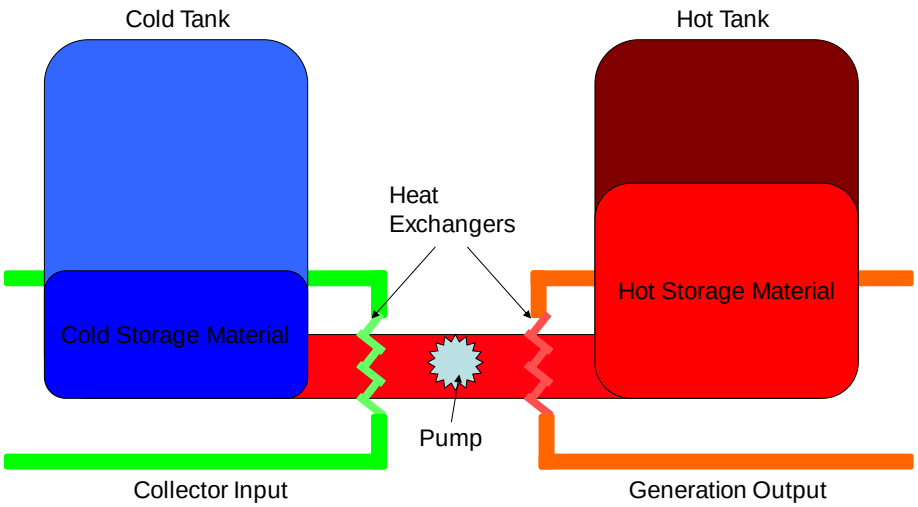

Figure 5: Diagram of a two-tank system, showing the system about half charged. Once all the cold material had been pumped through the collector heat exchanger, making it hot, the system would be fully charged.

The two-tank system is more complicated than a thermocline, and generally more expensive. The two-tank system requires a pump, a heat exchanger, and large quantities of the storage material. The thermocline is substantially cheaper than an equivalent energy storage capacity two-tank as the filler is used to reduce the quantity of storage material required. Since the filler is much cheaper than the storage material, the thermocline for a given energy storage capacity is cheaper. Filler is not used in a two-tank system as the filler cannot be pumped with the storage material without major design changes.

2.3.3 Brick

As the name suggests, a brick TES system uses a large solid block of material as the thermal storage material. In the brick TES system, the HTF transfers its energy into the storage material by being pumped through internal passages in the brick, and gradually warms the brick. The brick itself is generally made of concrete. Concrete serves as an excellent brick material due to its formable starting state, resistance to weather effects, and high specific heat. The formable starting state in particular is a significant advantage as it allows for internal structures in the brick, such as HTF tubes and internal truss structures with a higher thermal conductivity than the concrete. Current research has focused on improving the thermal conductivity of the brick to improve the input and output rates from such systems. Alternatively, some brick systems have incorporated encapsulated phase change materials to improve the total energy stored by the brick. Ideally, both methods could be used simultaneously.

The material used in this investigation, a nitrate eutectic, (which will be expanded on later) is generally used in either the two-tank system or the thermocline. The nitrate works best in those systems because it is kept as a fluid in both of those systems, and it has a high specific heat, allowing the systems to store significant quantities of energy in a given volume. The existing small-scale TES thermocline and two-tank systems predominantly use molten salts, with the nitrate being a commonly used storage material in those systems. The brick TES cannot use the nitrate as the primary storage material, as the nitrate would melt before storing much energy.

2.4 Existing Materials

The current standard thermal energy storage material is a nitrate eutectic, comprised of sodium nitrate and potassium nitrate. This material works fairly well, as it has a low melting temperature, a moderate specific heat, and a moderate thermal conductivity. The nitrate eutectic is meant to be used only in its liquid phase, and has been applied in thermoclines and two-tank systems for more than 40 years. Several variants of the basic form exist under trade names, such as Hitec solar salt and Hitec XL. The important physical properties of these composites are listed in Table 1.

Table 1: Reference thermophysical values for the Hitec Solar Salt by Coastal (1). As a point of comparison, water has a specific heat of 4.18 J/gK.

	Hitec Solar Salt	Units
Specific Heat	1.55	J/gK at 350C
Heat of Fusion	132.58	J/g
Melting Point	222	C

2.4.1 Standard Nitrate Eutectic

The standard nitrate eutectic compound chosen for this investigation has the industry name "Hitec Solar Salt", and is manufactured by Coastal Chemical. This particular eutectic is a blend of sodium nitrate ($NaNO_3$) and potassium nitrate (KNO_3), with a 55% $NaNO_3$ molar ratio blend. The eutectic diagram is shown in Figure 6. A eutectic is a fixed-ratio mixture of two or more materials that has a lower melting temperature than any other ratio of the mixture components. The Hitec eutectic provides close to the minimum melting temperature of any mixture of the two eutectic components. This is desired as the nitrate eutectic is not designed to function as a thermal energy storage material in both the solid and liquid phases, but rather functions exclusively in the liquid phase. Hitec is used in several existing facilities and is available in significant quantities for a low cost. The heat of fusion for various eutectic fractions is shown in Figure 7. The reference specific heat of the chosen nitrate eutectic is shown in Figure 8.

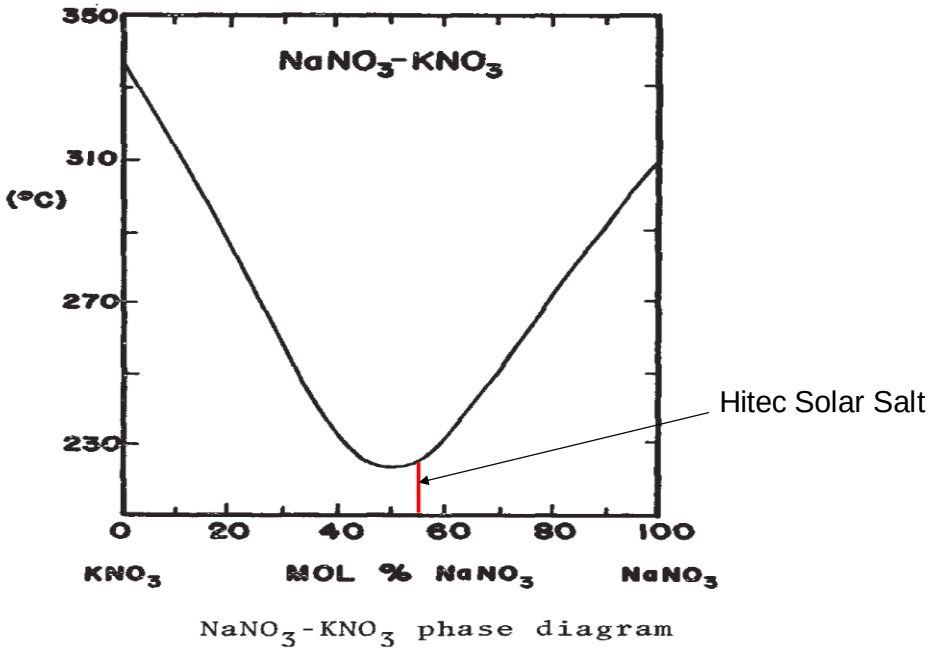

$NaNO_3$-KNO_3 phase diagram

Figure 6: Nitrate eutectic diagram by Janz *et al*. (2). The red line shows the mixture point of Hitec solar salt. The mixture point of Hitec is near the minimum melt temperature of any mixture.

Composition (mol % KNO_3)	ΔH_f° (kcal mol^{-1})	T_m (°C)
0	3.600	310
25	3.382	275
40	3.290	243
50	3.195	227
60	3.100	230
75	2.802	260
87	2.685	300
100	2.300	337

Figure 7: Heat of fusion for various nitrate eutectic mixes by Janz *et al*. (3). The Hitec solar salt mixture is at 55% sodium nitrate, so the heat of fusion is between the 50% and 60% mixture heat of fusion value.

T (K)	C_p (cal $K^{-1}mol^{-1}$)	T (K)	C_p (cal $K^{-1}mol^{-1}$)
510	39.99	650	36.29
520	39.72	660	36.03
530	39.46	670	35.77
540	39.19	680	35.50
550	38.93	690	35.24
560	38.67	700	34.97
570	38.40	710	34.71
580	38.14	720	34.45
590	37.88	730	34.18
600	37.61	740	33.92
610	37.35	750	33.66
620	37.08	760	33.39
630	36.82	770	33.13
640	36.56		

Figure 8: Reference specific heat values for a 50% sodium nitrate eutectic by Janz *et al*. (3). The Hitec solar salt is a 55% sodium nitrate eutectic, so the values will be slightly different.

The strengths of the nitrate eutectic are based around its use as a sensible-only thermal energy storage medium. The material is thermally stable for long periods in the liquid phase. The material has a low melting temperature of about 220 C. The material has a specific heat in the liquid phase of about 1.55 J/gK. The material is relatively cheap and available in large quantities, making potential manufacturing of a nanoparticle composite material an easier task. The eutectic components are generally non-toxic and non-flammable, so a spill or rupture would be less dangerous for the environment around a CSP facility. The material is highly soluble in water, making cleanup from a spill much easier, unless it is raining.

The weaknesses of the nitrate eutectic are more due to long-term operational concerns than thermal property issues. The eutectic has a relatively low decomposition temperature, observed to be around 500C, as shown by Peng *et al*.(4). The nitrate is highly corrosive, requiring additional maintenance and replacement. The material is hydrophilic, and will absorb water from the atmosphere if left in an open container.

2.5 Nanoparticle Augmentation

Many papers, a few of which will be referenced later, have been published in which the effects of adding nanoparticles to substances to change their properties are discussed. Many discuss how best to change the physical properties, such as strength or conductivity, others show how best to modify a fluid to suit its purpose best. In particular, there have been many studies on changing the thermal properties of water. The studies used to design this investigation have looked at changing the specific heat and the thermal conductivity of aqueous solutions by doping them with various concentrations of nanoparticles. These papers described a wide variety of tests to determine the thermophysical properties, but the overall view is that the addition of small concentrations of nanoparticles will significantly change the thermal properties of water.

2.5.1 Nanoparticle Selection

Research by others, such as Easterman *et al*. (5, 6), Wang (7, 8), Zhou (9,10), and Sundar (11)has shown that small additions of certain nanoparticle types seems to influence the thermophysical properties of water to a varying degree, based on the nanoparticle material and the concentration, using a variety of manufacturing methods. Using these publications, it was concluded that the best options for improving the thermophysical properties of the nitrate eutectic were alumina (Al_2O_3) and silica (SiO_2). The observed water thermal properties showed the addition of nanoparticles reduced the specific heat but increased the thermal conductivity. The drop in the specific heat is expected given the large disparity in the specific heat of water and the specific heat of the bulk material form of the nanoparticles. Additionally, others such as

Likhachev (12) and Wang (7, 8) have observed that the specific heat of nanoparticles of a given material can be significantly higher than the bulk form of the same material. Unfortunately, no specific papers were found that describe the specific heat of the nanoparticles, only the bulk material. The first instance in the literature showing experimental data for specific enhancement of nanofluids was by Nelson (13). The prior misconception in the nanofluids literature was that addition of nanoparticles results in the reduction of the specific heat of nanofluids. Subsequently repeatable and stable experimental data was reported showing the enhancement of specific heat of molten salts when doped with nanoparticles (14).

2.5.2 Mass Percentage Selection

A variety of published works (5, 6, 7, 8, 9, 10) have shown that there is an anomalously large effect at low nanoparticle mass concentrations when altering the thermal properties of a base material. For water, these values typically range between 0.1% and 5% by volume. To simplify the testing process, a mass percentage was chosen instead and set to 1%.

2.6 Malik Thesis Comparison

The most applicable previous work was a thesis written by Darren Malik, of Texas A&M. (15) His thesis also dealt with increasing the specific heat of thermal energy storage fluids, specifically the nitrate eutectic used for the present investigation in this thesis. The author of this thesis worked with Darren Malik on his thesis. This investigation is an extension and improvement on Darren Malik's experiments based on additional work, observations, and improved methodologies.

2.6.1 Materials

Malik's work was focused on the same nitrate eutectic, but only used alumina nanoparticles. In addition to testing silica nanoparticles, alumina nanoparticles were used a second time to show any effects of a modified manufacturing method, detailed later. The same source of raw nitrate eutectic was used to eliminate any variability from the source.

2.6.2 Pak and Zhou Models

Malik's work showed these models to be poor indicators of specific heat of nitrate/nanoparticle combinations. Several significant differences between the Pak/Zhou experimental setup and Malik's setup could account for the failure of those models. The largest difference is the base material used to prove or disprove the model. Pak/Zhou tested water and nanoparticle combinations, rather than a molten salt and nanoparticle combinations. This change manifests in several important ways. In the Pak/Zhou model, the mixture components had highly dissimilar bulk specific heat values. The nitrate and nanoparticle material bulk specific heat are very similar. The nitrate salts are significantly more dense than water, which would alter the nanoparticle suspension and dispersion properties of the mixture. The testing temperatures of the nitrate mixture are far higher than the water mixtures tested in the Pak/Zhou models.

2.6.3 Manufacturing Method

Malik used a slightly different manufacturing method than was used in this investigation. While Malik also prepared his samples using both dry mixing and an aqueous

solution and sonically mixed the solution to promote nanoparticle dispersion, several small factors were changed in the mixing and drying phases of material preparation for this thesis. The largest difference is the temperature at which water was removed from the mixture. Malik used a high temperature to promote rapid water removal. The reason for minimizing the removal time was to prevent nanoparticle re-agglomeration. However, observations suggest boiling promotes re-agglomeration by forcing rapid internal fluid motion, undoing the dispersion of the sonic mixing. Therefore, the method used in this investigation was modified to address this observation by avoiding boiling by reducing the temperature of the hot plate used to speed up the water removal process. Large quantities of desiccants were placed near the evaporating aqueous mixture to further aid water removal.

2.6.4 Nanofin Issue

Malik proposed the gradual decline of his specific heat measurements was due in part to a build-up of nanoparticles on the testing equipment, specifically the platinum sample pans used in DSC testing. Current cleaning methods were insufficient to purge the pans of all nanoparticles, leading to the possibility of nanoparticle buildup on the pans compromising the result set. To combat this, all testing done for these experiments was performed using disposable hermetically-sealed aluminum pans. Only using the pans for a single sample and a limited number of runs ensures no nanoparticle buildup on the DSC or the pans, as each sample used a new pan. This method also precludes the possibility of nanoparticle cross-contamination. Lastly, the aluminum pans used were hermetically sealed, so no material could leave the pans after they were sealed, unlike the platinum pans used in Malik's thesis. Malik's

pans were vented and used an unsealed lid, so the sample material could push the lid off or escape the pan entirely. Using the aluminum hermetic pans, the only way this could happen was if there was a structural failure of the pans due to internal pressure, which would invalidate the test.

2.6.5 Measurement Technique

Malik's experiments used the ASTM 1269E method exclusively. This method is comprised of several steps, and is therefore more susceptible to experimental error than the MDSC method, explained later in this thesis. To reduce measurement uncertainty, this thesis used the ASTM and MDSC methods to find specific heat information. The ASTM method was still used to allow for a direct comparison between Malik's results and the results found for this thesis. The ASTM method is also valid over the full testing temperature range, while the MDSC method had to be proven to work correctly at elevated temperatures to be used in this thesis. A side benefit of the MDSC method is the ability to observe the heat of fusion with the specific heat through a phase change due to the slow ramp rate required by the method. The ASTM method requires too high a ramp rate to accurately determine the heat of fusion during a ramp, requiring a break in the data if the heat of fusion is needed.

2.6.6 Temperature Profile

A significantly different temperature profile from that used by Malik was used to determine the thermophysical properties of the samples. The experimental thermal profile will be discussed in more detail later in the method section, but there are several key differences

between the thermal profile used by Malik and the profile used in these experiments. First, the thermal profile used in this thesis included a pre-measurement temperature “spike”, designed to melt the sample before specific heat information was taken and to condition the test machine. The “spike” also ensured the sample was a solid during specific heat measurements, rather than a powder. Next, multiple data segments were taken of each sample using a single thermal profile, rather than a single valid temperature ramp. Lastly, to minimize the sample geometry-changing effects of a phase change, the number of phase changes was minimized during specific heat testing by keeping the nitrate in the liquid phase for the duration of the specific heat measurements. Lastly, a different class of measurement device was used in this investigation; Malik used a thermogravimetric differential scanning calorimeter, whereas a true differential scanning calorimeter was used in this investigation. Thermogravimetric differential scanning calorimeters are more frequently used for determining chemical stability and chemical reaction rates due to their ability to observe the mass of a sample while changing the temperature of the sample.

3. METHOD

The overall experimental method was to create a homogenous powder nanoparticle composite material, then test its thermal properties using a Differential Scanning Calorimeter (DSC).

3.1 Nanomaterial Fabrication

To create the nanoparticle composite materials, several steps were taken, using previous work (2) as a starting point. The first generalized step is combination, second is mixing, and third is water removal. The nitrate eutectic components are highly hydrophilic, so the material was prepared in a dry, Argon-filled glovebox. Later steps require the material to be in an aqueous solution, so the components were massed, then combined in distilled water to form the base aqueous eutectic. The base eutectic was purchased in the form of pre-mixed pellets, so these were crushed into a powder using a mortar and pestle into a fine powder before being added to distilled water. The solubility of the nitrate eutectic mandated a ratio of 10 mg per mL of solution. The chosen nanoparticles were alumina (Al_2O_3) and silica (SiO_2), and were added to the aqueous solution of the base eutectic. The nanoparticles were added such that they comprised 1% of the mass of the eutectic in the aqueous solution.

In order to ensure complete distribution of the nanoparticles into the eutectic, the aqueous solution had to be sonically-mixed for a set duration of 2 hours, as that was both the observed minimum time to dissolve the nitrate in the solution fully and qualitative observations suggest additional sonication will re-agglomerate the nanoparticles. Based on the limitations of

the sonic mixers used, the standard batch size was about 2g of composite material, as the largest standard container held 200 mL of water. This batch size was used to minimize the number of batches required to make sufficient test material for all the experiments. A larger batch size was found to be impractical, as the larger container required reduced the effectiveness of the sonic mixing and extended the drying time, which will be discussed next.

Once this mixing was done, the material was transferred back to the glovebox. Once in the glovebox, the sample mixture was heated in a steel pan on a hot plate set to 90 C, so the water would quickly evaporate out of the pan without actively boiling, leaving the nanoparticle composite material as a precipitate in the steel pan. To ensure the water would not simply be taken in again by the eutectic, several trays filled with desiccants were placed in another portion of the glovebox. This setup was maintained until all the water was driven from the steel pan, and a fine-grain white powder was left coating the bottom of the steel pan. Since the material was precipitated out of the aqueous solution, it adhered to the steel pan, so it had to be removed physically. To accomplish this, a steel paint scraper was used to scrape the material from the pan, leaving a loose, white powder with a consistency of flour. The white powder was the final testing form of the nanoparticle composite eutectic. The material was then transferred from the pan to a container for later use, and stored in an oven at 140 C to ensure the processed material would not absorb water while in storage.

The use of nanoparticles created several significant challenges in the area of sample preparation. The largest challenge stems from the small size of the nanoparticles: cross-contamination. In order to prevent cross-contamination, all samples were prepared in a cleaned glovebox, and each nanoparticle type had its own tool set, meaning there was a steel pan and scraper used only for silica nanoparticles and another set used exclusively for alumina.

This procedure was followed to ensure minimal cross-contamination, as even with extensive cleaning, nanoparticles tend to remain on surfaces and tools they come in contact with. A secondary concern was water absorption by the prepared samples. The thermal testing method requires little to no water in the sample material to ensure accurate results and to prevent machine damage. To prevent water absorption, the samples were kept in the dry glovebox, and before being used in the thermal analysis machine, the samples were heated in a vacuum furnace up to 140 C for at least a day.

The thermal properties of the nitrate composite materials were found using several different methods. ASTM 1269E and MDSC testing were used to determine the specific heat. A secondary measurement of the heat of fusion was also performed, as the heat of fusion measurement could be added to the specific heat determination with a minimum of time and effort.

3.2 Differential Scanning Calorimetry (DSC)

DSC is a thermal property determination technique, and also a device based on that technique. The technique uses a device called a differential scanning calorimeter. The general operating principle of the device is to compare the thermal energy input into two samples simultaneously. One sample is called the reference; the other is the actual sample to be measured. The standard setup is to make the reference an empty sample containment pan, and the measurement specimen is the unknown material in a sample containment pan. The recorded data output, usually called the heat flow, is the reference thermal energy input minus the sample thermal energy input to create a single value which represents the difference in

energy required to raise the temperature of the sample and reference items by the same quantity. The thermal energy difference between the sample and reference specimens is the energy required to raise the temperature of the unknown specimen by the same amount, as the energy required to raise the sample pan temperature is accounted for by the reference heat flow signal. There are two primary data outputs for standard DSC: heat flow and temperature. There are two methods to get the specific heat from this information: ASTM 1269E and MDSC.

3.2.1 ASTM 1269E Testing

ASTM 1269E is the most widely accepted means of determining the specific heat of an unknown sample using a DSC. A sample measurement is comprised of three separate measurements: a baseline, a sapphire, and the sample. The baseline measurement is required to compensate for any miscalibration of the machine and any sample/reference pan mass differences. The sapphire run is used to determine the power required to heat a very well-characterized material, as the specific heat of sapphire is known over a wide temperature range with high accuracy. The sample run is then compared to the sapphire run after factoring in for mass differences between the sapphire and the sample. The temperature profile used with the ASTM 1269E method is shown in Figure 9. The described method results in 3 liquid phase measurements, and heat of fusion measurements can be added after the specific heat measurements using the standard testing procedure outlined in ASTM 1269E,which is discussed in more detail later. These repeat measurements in the profile were done to ensure the reported values for a given sample were repeatable. Each of the repeat measurements was

called a cycle, as the profile makes the DSC cycle through the same temperature range several times. Cycle 1 was the first measurement, cycle 2 was the second, and cycle 3 was the third.

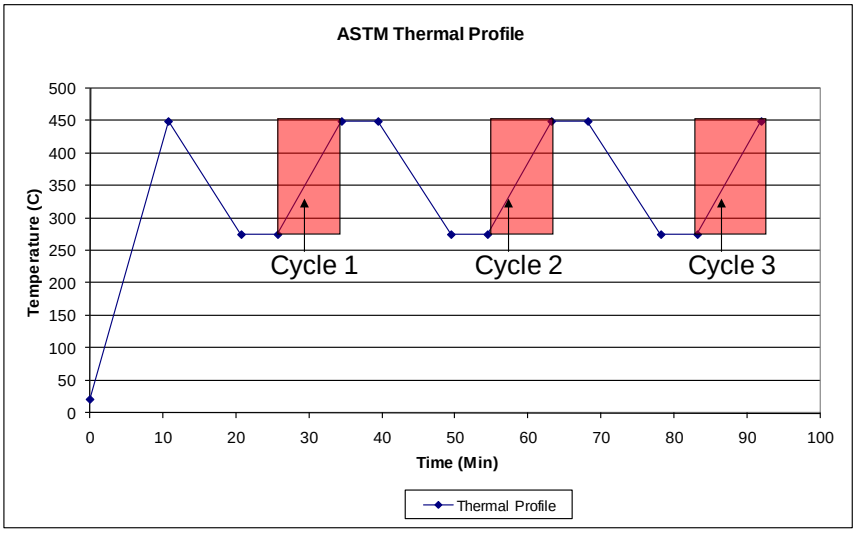

Figure 9: ASTM 1269E test temperature profile. The first temperature increase segment is called the "spike", as it is designed to melt the sample, rather than measure data. The other three increase segments are temperatures where data used to determine specific heat is taken.

ASTM 1269E uses a series of equations, described below, to convert the heat flow signal from the DSC into the specific heat of the unknown sample. The equations use the results of all three runs previously mentioned (the baseline, sapphire, and sample runs) to determine the specific heat.

$$D_S(T) = S(T) - B(T) \tag{1}$$

$$D_R(T) = R(T) - B(T) \tag{2}$$

$$C_{PS}(T) = C_{Pr}(T)\left(\frac{D_S(T)\cdot M_R}{D_R(T)\cdot M_S}\right) \tag{3}$$

In Equation 1, D_S is the corrected heat flow of the sample at a temperature, S is the heat flow of the sample at a given temperature, B is the baseline heat flow at a given

temperature, and $M_S$is the mass of the sample. In Equation 2, D_R is the corrected heat flow of the reference at a given temperature, $R$is the heat flow of the reference at a given temperature, and M_R is the mass of the reference. In Equation 3, $C_{:Ps}$is the specific heat of the sample at a given temperature, and $C_{Pr}$is the specific heat of the reference at a given temperature. This equation set is sometimes referred to as the ratio method. There is a provision in ASTM 1269E to include the effects of pan mass on the computed specific heat, but due to the requirements of the MDSC method, the pans were mass matched for the ASTM tests as well. This negated the need to apply the more complicated ASTM 1269E method, and allowed the use of Equations 1, 2, and 3 their place.

3.2.2 MDSC Testing

An alternative method to find the specific heat of a sample was Modulating Differential Scanning Calorimetry (MDSC). This method was created by Thermal Analysis, (TA) a DSC designer and manufacturer, and their Q200 and Q2000 DSCs support this option. This method superimposes a sinusoidal temperature variation over a fixed temperature increase rate. Using the sinusoidal temperature response of the sample and reference pans, the specific heat of the sample can be found. The applicable ASTM standard is ASTM E2716, and was followed where allowable. While the ASTM 1269E method can be run on any DSC, including a MDSC, the MDSC method can only be run on a suitable TA DSC with the MDSC option, as the MDSC method requires a different set of sensing hardware to detect the minimal changes in temperature and heat flow. The additional hardware and internal calculations give the MDSC method additional

outputs over the standard ASTM 1269E method. The MDSC method has a direct data output of heat flow, temperature, and specific heat.

To verify the accuracy and precision of the MDSC method at the required temperature range, a series of tests were performed using the standard DSC calibration sample material, sapphire. A single sapphire sample was placed in the sealed hermetic aluminum pans used for the nitrate tests. The temperature profile for the sapphire runs was determined by thorough review of TA's documentation and internal testing of the method. A standard MDSC test temperature profile can be seen in Figure 10. The sapphire sample was run four times to determine the precision and accuracy of the MDSC method. The results of these tests can be seen in the MDSC High Temperature Validation Results section, which clearly shows that the method is both highly accurate and highly precise. A more thorough analysis is presented later, in the Results section.

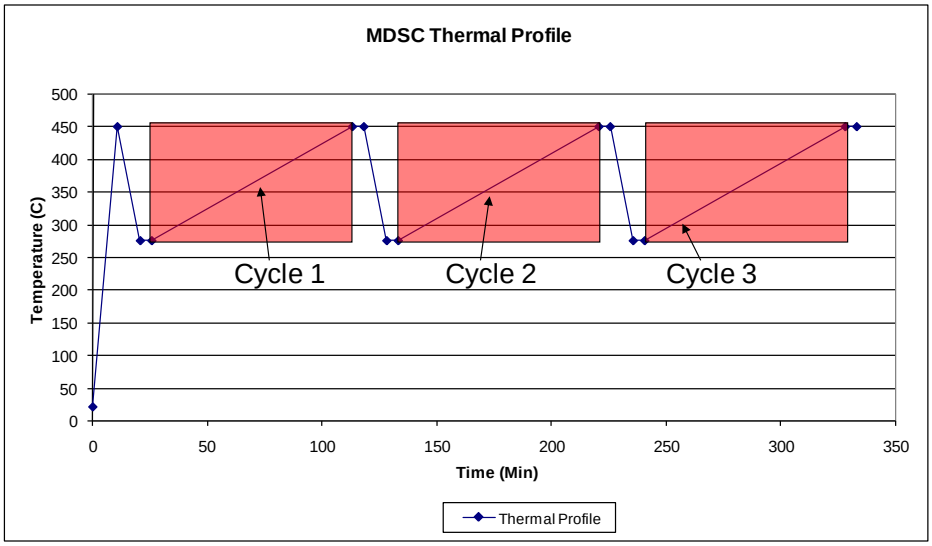

Figure 10: MDSC temperature profile. Like the ATSM temperature profile, there are four temperature increase segments, three of which are used to gather specific heat data.

Due to the superbly accurate and precise measurements obtained using the MDSC method with the sapphire samples, testing was extended to the nitrate eutectic, but with modifications. In particular, the measured temperature range was reduced, as the CSP system operational temperature range is only from approximately 300 C to 600 C. The modulation was set up with a 1C amplitude and a 120 second period. The method was created to minimize the phase change effects in the run data while still allowing for data collection during a phase change to find the heat of fusion after the specific heat measurements had been taken. The multiple repeats in the liquid phase allows for confidence in the data for a particular sample, as there are three measurement repeats in the liquid phase. Preliminary, qualitative testing showed minimal changes in the sample distribution within the sample pan after multiple freeze/melt cycles, but multiple heat of fusion measurements were still taken after the specific heat measurements.

3.2.3 ASTM 1269E Comparison with MDSC for Specific Heat

The ASTM 1269E and MDSC methods determine the same thermophysical property, specific heat. Both methods compare a sample to an established standard to determine the sample's specific heat. However, one of the key differences between the two methods is duration. In the ASTM 1269E test, the sample is only at any given temperature for a relatively short span of time, due to the high ramp rate required by the method. In comparison, the MDSC method uses a very slow ramp rate, therefore any thermophysical changes that occur over time at elevated temperatures are far more likely to occur with the MDSC method. A significant question with the composite nanomaterial is if the nanoparticles will precipitate out

of solution or agglomerate, as both of those occurrences will negate any positive benefit the nanoparticles gave to the material. This event is unlikely to occur fast enough to be captured by the ASTM 1269E method, but it may impact the results of the MDSC method. Therefore, both methods were used to determine the specific heat.

3.2.4 Heat of Fusion Measurement

The heat of fusion, according to ASTM 1269E, is the definite integral of the heat flow with the limits of integration being the onset and offset temperature of the melting sample while the temperature ramp rate is extremely low, 2 C per minute. The extremely low ramp rate is required to minimize the impact of the specific heat term of the total instantaneous energy absorption equation, shown as Equation 4.

$$Q = m(C_p \Delta T + H_f) \tag{4}$$

In Equation 4, $Q$is the heat flow into the sample, $C_p$is the specific heat of the sample, $\Delta T$is the change in temperature, $m$is the mass of the sample, and $H_f$is the heat of fusion. As can be seen from Equation X, the smaller the ΔT, the smaller the effect on Q the C_p has. A low ramp rate reduces ΔT, so the best way to find the heat of fusion is to ramp through the melting temperature range as slow as possible so the energy absorbed, Q, will be almost entirely due to the heat of fusion.

Table 2: Total minimum required experiment list. The time required to perform each test varies with the temperature range required and the testing method, as the ASTM and MDSC tests require different amounts of time for the same temperature range.

Material	# of tests	hours per test
Plain Nitrate	6	6 to 9
Nitrate + Silica	6	6 to 9
Nitrate + Alumina	6	6 to 9

The total required test list is shown in Table 2. Three sample runs of each type were used, requiring months of testing. A minimum of three repeats were chosen to reduce time required for testing and to reduce cost, while still allowing for sufficient data integrity. All materials of the same type were from the same material creation batch, in order to ensure consistency between the samples. A minimum of 6 runs were required for each material to allow for three repeat measurements of each tested method and property: three ASTM measurements and three MDSC measurements.

3.3 Stability Determination

As stated in the introduction, one of the objectives is to determine if the nanoparticle composite material is thermally stable. While there is an ASTM test to determine the thermal stability of a sample using DSC (ASTM E537-07) the type of thermal stability being determined by that testing method is different from the thermal stability desired in these tests. ASTM E537-07 looks at chemical reactions due to temperature and environment, and uses the heat flow to determine if a reaction takes place. For the purposes of this investigation, thermal stability refers to the consistency of the specific heat over the test duration, rather than the thermally-

triggered reactivity of the sample. There is no established testing method for this sort of observation. Therefore, the quantifiable metrics will be established here.

As described in the ASTM and MDSC method sections, the temperature profiles used in determining the specific heat consist of multiple repeats of the same ramp rate and temperature range. The temperature profile takes a considerable amount of time to completely execute due to the fixed temperature ramp rates and the time to cool the instrument between measurement cycles. While this length of time is a far less than a dedicated thermal stability test designed to emulate the operational thermal profile of a thermal energy storage system, it is still useful as a possible measure to determine if the nanoparticles are falling out of solution, as if they are, the specific heat should decrease over time as the nanoparticles coat the lower surface of the sample pan, reducing the concentration of nanoparticles suspended in the sample.

The way to quantify the decrease in the specific heat over time is to compare the measured specific heat from multiple cycles at a fixed temperature. The progressive change over time will be shown as a percentage change of the specific heat from cycle to cycle for a fixed temperature. Therefore, for the temperature profiles previously discussed, there will be two measurements of the stability for each sample: a percentage change in the specific heat between the first and second measurement cycle, and a percentage change in the specific heat between the second and the third measurement cycle. A consistent decrease will manifest as two negative percentage changes greater than the measurement uncertainty of the DSC. Other possible outcomes represent unclear results, as many other factors could cause an apparent increase in specific heat between cycles, such as a material or sample pan geometry change.

4. RESULTS AND DISCUSSION

4.1 MDSC High Temperature Validation Results

As discussed in the Method section, the MDSC method is still relatively new, and used exclusively with TA products. Therefore, a series of validation runs were performed to demonstrate the accuracy of the MDSC method using the parameters listed in the Method section. Since the method used was MDSC, the raw output was specific heat, in J/gK. The temperature profile used was slightly modified from the standard sample profile listed in the Method section, as it contained only one measurement cycle and the initial “spike” ramp segment. All tests were performed with the same sapphire sample, but were run on different dates with different pan pairs, in order to emulate standard MDSC test runs using different samples. Four such tests were performed, with two tests using a temperature range of 100C to 600C, the other two ranging from 300C to 600C. The specific heat results are shown in Figure 11, with the error compared to reference values shown in Figure 12. While the sapphire specific heat data was taken over a wider range than shown in the figures, the accuracy at temperatures lower and higher than the nitrate thermal profile measurement cycles is irrelevant to this investigation, and was therefore not shown. The error was found by calculating percentage difference between the reference and observed specific heat.

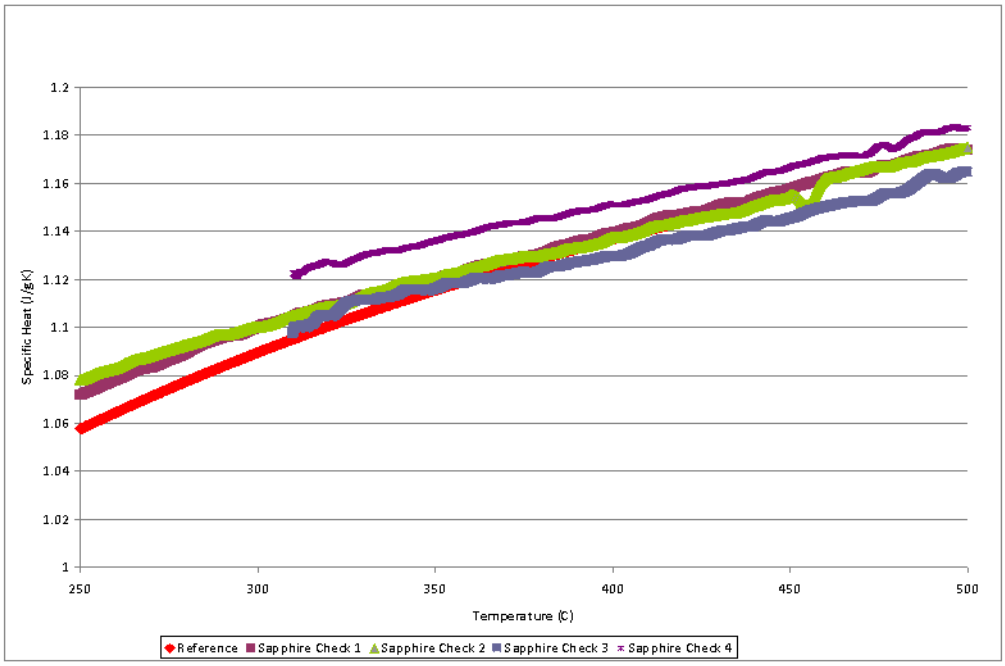

Figure 11: MDSC observed sapphire specific heat. The observed specific heat matches very closely to reference values.

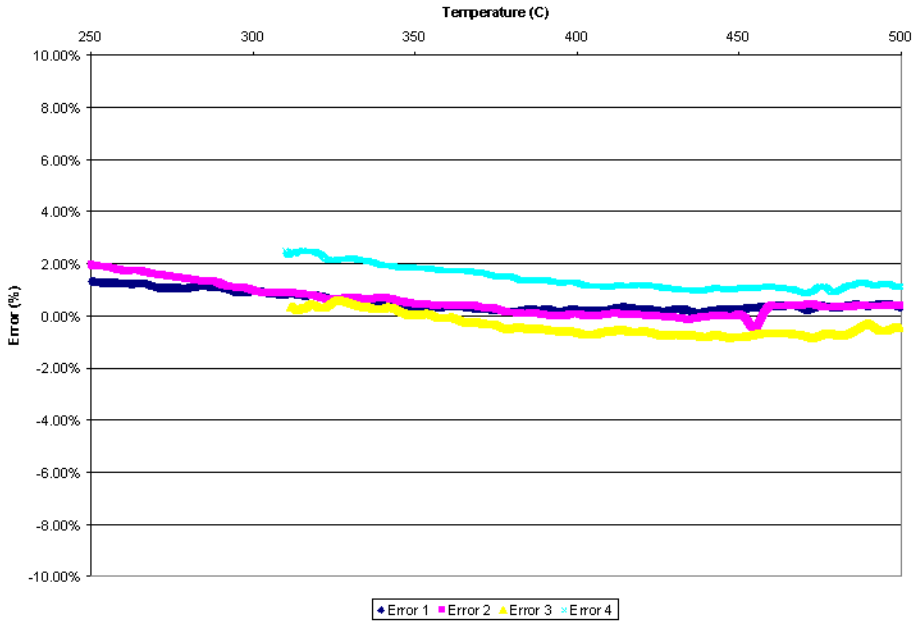

Figure 12: Observed sapphire MDSC error, showing an average error of approximately 2-3%.

Based on the observed error shown in Figure 12, a standard uncertainty range of approximately 3% seems to be sufficient to encompass most of the observed error. The observed error is within the manufacturer's specifications of 5% error. There was a large initial error was present in every MDSC measurement, and MDSC parameter testing not included in this investigation showed it to be a time, rather than temperature, based effect. Therefore, MDSC measurements require a certain amount of "settling time" to come to the true observed value. The large initial error seems to be inherent to the MDSC method, as every MDSC test performed, regardless of the material or parameters used, showed the same initial error spike.

The MDSC method using the parameters discussed in the Method section showed superb correlation with expected reference values, and showed an average error below 2%. This performance allows for great confidence in the MDSC specific heat results outside the ASTM E2716 temperature range. The specific heat accuracy also suggests the MDSC settings as described in the Method section were optimal for the pan and temperature range used in this investigation.

4.2 Specific Heat Results

The summarized results are shown in Table 3. The data was taken using measurement techniques as described in the Method section. A sample consists of one mass-matched reference and sample pan set, and the contents of the sample pan, which was the material being tested. The temperature profiles given in Figure 9 and Figure 10 show a total of four temperature ramps. The first ramp, as mentioned in the method section, is to melt the sample into a solid and condition the machine. The other three ramps are the measurement cycles to

gather the data. A run consists of the data gathered from executing the temperature profile once. The specific heat values shown in Table 3 are the averaged values from each of the three measurement cycles for each sample. The heat of fusion measurements were taken after the specific heat measurements, in order to prevent geometry effects (as the material freezes and melts) from altering the specific heat data.

Table 3: Summarized specific heat and heat of fusion results for all tests.

Test Number	Nanoparticle	Measurement Type	Maximum Temperature	Sample Mass	Cp at 350C Average	Heat of Fusion Average
Units			C	mg	J/gK	J/g
1	none	ASTM	450	12.62	1.54	n/a
2	none	ASTM	450	8.66	1.61	n/a
3	none	ASTM	450	18.57	1.59	n/a
4	none	MDSC	400	10.20	1.57	87.84
5	none	MDSC	400	11.00	1.46	88.37
6	none	MDSC	450	7.21	1.54	101.50
				avg	1.55	92.57
7	alumina	ASTM	450	6.48	2.07	n/a
8	alumina	ASTM	450	7.10	1.90	n/a
9	alumina	ASTM	450	17.47	1.80	n/a
10	alumina	MDSC	450	9.86	varies	n/a
11	alumina	MDSC	450	7.94	1.81	97.29
12	alumina	MDSC	450	10.45	1.73	101.27
13	alumina	MDSC	450	8.56	1.91	99.59
14	alumina	MDSC	450	8.20	1.84	103.77
				avg	1.87	100.48
15	silica	ASTM	350	5.18	1.91	n/a
16	silica	ASTM	400	9.77	2.00	n/a
17	silica	ASTM	450	10.44	1.76	115.73
18	silica	MDSC	450	7.26	varies	n/a
19	silica	MDSC	425	9.41	varies	n/a
20	silica	MDSC	400	9.77	n/a	n/a
21	silica	MDSC	400	9.77	1.84	97.62
22	silica	MDSC	400	10.23	1.72	91.43
23	silica	MDSC	400	12.99	1.82	95.56
				avg	1.84	100.09

The statistical analysis of the data in Table 3 is shown in Table 4. The average values in Table 4 were generated using the data from both methods for each material. The standard deviation was generated in the same way, using all the data for each material type. The 90% confidence interval was generated using the standard deviation given in the first column of Table 4, and the maximum and minimum were created using the 90% confidence interval data.

Table 4: Statistical analysis of the data from Table 3, showing the 90% confidence interval and standard deviation.

	Average Value	Standard Deviation	90% Confidence Maximum	90% Confidence Minimum
Heat of Fusion	J/g	J/g	J/g	J/g
Nitrate	92.57	7.738	105.3	79.8
Nitrate + Al_2O_3	100.48	2.734	104.9	95.9
Nitrate + SiO_2	100.09	10.744	117.8	82.4
Specific Heat at 350C	J/gK	J/gK	J/gK	J/gK
Nitrate	1.55	0.050	1.63	1.47
Nitrate + Al_2O_3	1.87	0.108	2.04	1.69
Nitrate + SiO_2	1.84	0.103	2.01	1.67

Each run's individual specific heat temperature trace can be found in Appendix A. The averages of each material's specific heat values over the temperature range are shown in Figure 13. The data presented in the figures was generated by both the ASTM 1269E calculations as presented in the Method section and for MDSC results as a direct output of the DSC. The results of both methods were then plotted against temperature to generate Figure 13. Figure 14 shows the same data as presented in Figure 13, but presents it as a ratio against the

base nitrate. A value greater than 100% indicates the specific heat is higher than the base nitrate. As can be seen in Figure 14, the specific heat of the composite materials is always higher than the base nitrate.

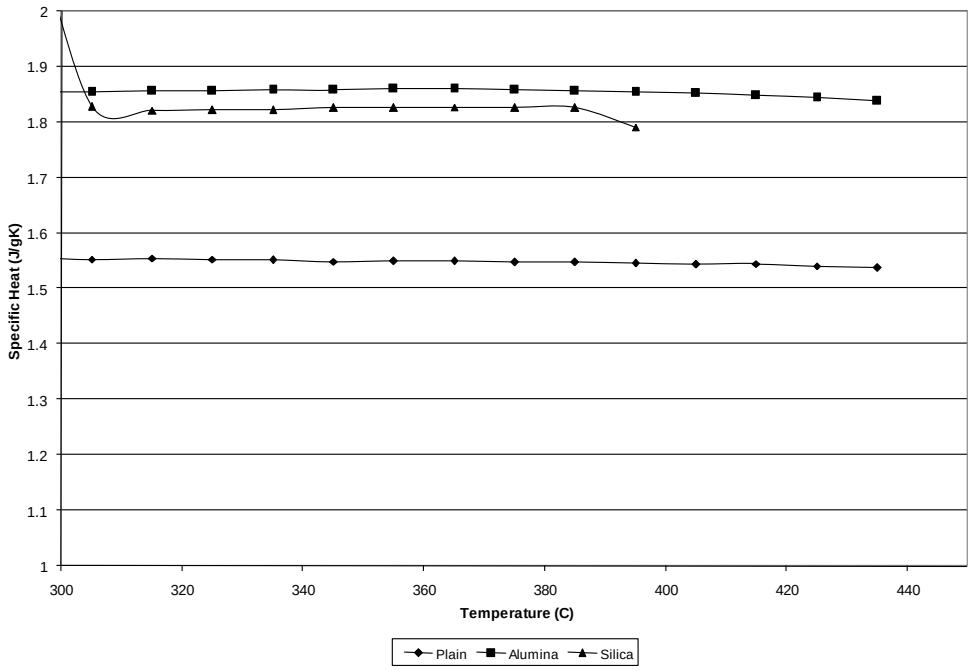

Figure 13: Specific heat results for all tested materials. These results are the averages of all tests at specific temperatures. The composite materials always showed a higher specific heat than the plain nitrate.

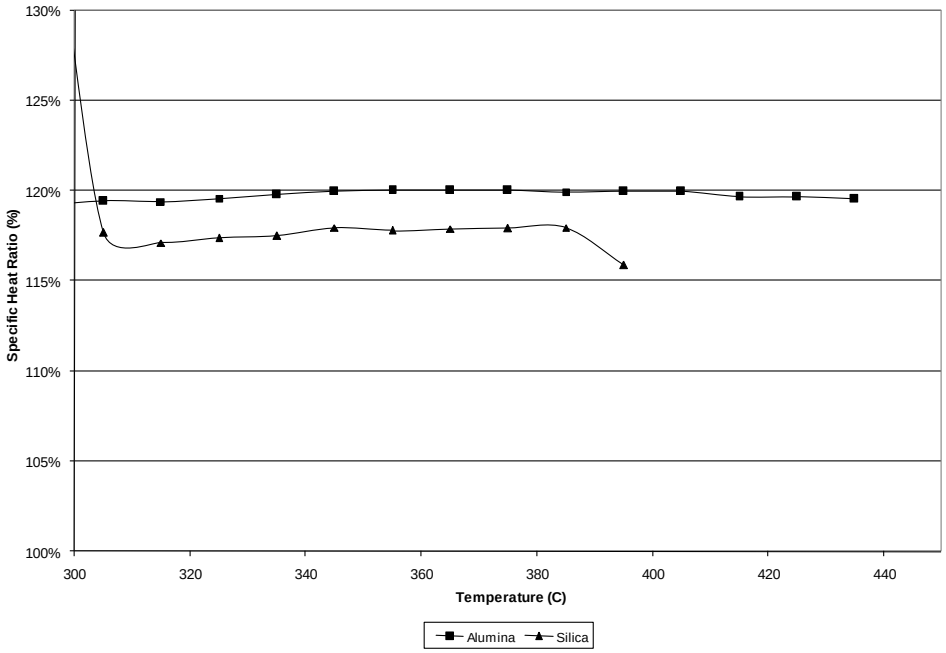

Figure 14: Specific heat ratios of all tested materials. This plot shows the specific heat ratio between the composite and base material at investigated temperatures. In this plot, the base nitrate always has a value of 100%. The composite materials always showed at least 15% improvement in specific heat compared to the base nitrate.

The ASTM and MDSC specific heat results for each material are shown in Table 5. These results were generated using the data shown in Table 3. Each material's method-specific data was used to generate the data in Table 5, meaning, for example, that the ASTM standard deviation for the plain nitrate was generated only using ASTM 1269E plain nitrate results, listed as runs 1, 2, and 3 in Table 3. The other table entries were generated in the same manner. The enhancement percentage was found by comparing the specific heat results of the composite nitrate against the plain nitrate.

Table 5: ASTM and MDSC specific heat statistics. The observed specific heat enhancement for both methods is approximately the same. The MDSC had lower standard deviation results than ASTM for almost all runs.

	ASTM			MDSC		
	Average	Standard Deviation	Enhancement	Average	Standard Deviation	Enhancement
Nitrate	1.58	0.037	0.0%	1.52	0.053	0.0%
Nitrate + Al_2O_3	1.93	0.116	22%	1.82	0.073	20%
Nitrate + SiO_2	1.89	0.122	20%	1.80	0.068	18%

The overall specific heat results shown in Table 3 and Table 4 support the hypothesis that the addition of nanoparticles improves the specific heat capacity. The exact degree of improvement is unclear, as evidenced by the standard deviation values shown in Table 4. Based on the average values, the nitrate and alumina showed approximately equivalent enhancement of the specific heat as the nitrate and silica. The results are a combination of MDSC and ASTM methods, and both methods provided similar results. The combined method improvement values are shown in Table 6, and are taken from Table 3.

Table 6: Combined Specific heat enhancement percentage. Note that the enhancement for both materials is approximately the same.

Material	Specific Heat Average	Enhancement
	J/gK	%
Nitrate	1.55	n/a
Nitrate + Al_2O_3	1.87	20%
Nitrate + SiO_2	1.84	19%

The exact quantity of enhancement is somewhat open for interpretation, given the 90% confidence interval range as seen in Table 4, but the same data suggests there is a clear enhancement, based on the 90% confidence interval range. The average values presented in Table 6 were determined using both methods to provide a wider range of data to pull from.

4.2.1 ASTM and MDSC Result Comparison

Both the ASTM and MDSC methods provided specific heat data within one standard deviation of the reference value for the plain nitrate, as can be seen in Table 5. This suggests that both methods were accurate at the temperatures for the tested materials. However, for the nanoparticle composite materials, the two methods provided specific heat information outside of one standard deviation relative to the average of the other for the same material. Each method's average is within the other method's 90% confidence interval, however, suggesting the two methods provide at least similar data. The other disparity between the two methods is in their standard deviations. The MDSC standard deviations are, with the exception of the plain nitrate, smaller than those of the ASTM method. This suggests the MDSC method has lower uncertainty than the ASTM method, at least under the conditions outlined in the Method section. A potential additional uncertainty source is the multi-step nature of the ASTM method. Since the method is comprised of three individual runs, the sample pan must be removed and placed on the sensor three different times, compared to the single time required by the MDSC method. A second possible reason for the higher uncertainty stems from the use of the hermetic pans. The hermetic pans must be crimped shut once the sample is inside. However, since the ASTM method requires the use of the same pans with different samples

(nothing, sapphire, and unknown sample) the pan could not be sealed until the unknown sample was put in the pan. Therefore, the pan may have behaved differently during the sample run compared to the previous runs.

The larger question is which method is closer to the actual specific heat of the composite materials. The ASTM method always gave higher specific heat results than the MDSC method for the composite materials. It then becomes a question of which method is more accurate. The ASTM method has been verified and used for many decades, while the MDSC method is still relatively new. The MDSC method is also not approved by the ASTM committee for the same temperature range used in this thesis. The MDSC method has been shown to be valid at the tested temperatures using sapphire standards tested under the same conditions as the unknown samples, as seen in Figure 11. The ASTM method internally validates itself by re-calibrating itself in every run. Therefore, it could be concluded that both methods are valid, even though they give different results. With this in mind, the approximate specific heat enhancement for both of the composite materials is 20%, as shown by both the ASTM 1269E method and the MDSC method.

4.3 Heat of Fusion Results

The heat of fusion results and statistical analysis are shown in Table 3 and Table 4. The heat of fusion measurement, as described in the Method section, is the definite integral of the heat flow, with the integration limits of the onset to the offset temperature of the melt. The heat of fusion measurements were taken after specific heat data was taken. The heat of fusion measurements were taken only during the MDSC runs because the ramp rates required by the

heat of fusion measurement match those required by the MDSC specific heat measurement. The observed heat of fusion is significantly lower than the reference value given by the base material manufacturer. The reason for this alteration is unknown. If the observed heat of fusion of the plain processed material is considered a baseline value, then the nanoparticle composite materials do not seem to have a significantly altered the heat of fusion.

4.4 Stability Results

As described in the Method section, determining the stability of the specific heat is the tertiary objective of this thesis. The stability was determined by comparing the specific heat at a given temperature between successive measurement cycles. A stable mixture will show a small change between cycles, lower than the machine's uncertainty. An unstable material will show a significant change in the specific heat between cycles. Each material has its own table, shown in Table 7, Table 8, and Table 9. These tables were generated by the procedure described in the Method section. All specific heat values were taken at 350C, and all tables used the same runs from Table 3.

4.4.1 Plain Nitrate Stability Results

Table 7: Plain nitrate stability analysis. The plain nitrate was shown to be stable, as the cycle to cycle changes were within the DSC's uncertainty.

Nitrate			Temperature	Mass	cycle 1	cycle 2	cycle 3	cycle 1->2	cycle 2->3
Run Number	Method	Date	C	mg	J/gK	J/gK	J/gK	%	%
1	ASTM	8/10/2010	450	12.62	1.512	1.545	1.550	2.18%	0.32%
2	ASTM	8/16/2010	450	8.66	1.583	1.616	1.619	2.08%	0.19%
3	ASTM	8/30/2010	450	18.57	1.580	1.588	1.591	0.51%	0.19%
6	MDSC	9/28/2010	450	7.21	1.544	1.536	1.533	-0.52%	-0.20%

Based on the previously established stability criterion, the nitrate was stable up to 450C, as all the cycle-change analysis showed, at worst, a change below 1%, which is well within the uncertainty of the DSC, which, as established by the test sapphire runs, is approximately 3%. The other runs all showed a per-cycle difference of no more than 2.5%, so there was no significant shift in the specific heat over the run duration. As seen in Table 7, Runs 4 and 5 are not present. This is because those runs did not have the multiple cycles of other runs, but were valid specific heat tests of the plain nitrate using MDSC under the same conditions as the other tests.

4.4.2 Nitrate + Alumina Stability Results

Table 8: Nitrate + alumina stability analysis. The nitrate + alumina was stable in nearly every test.

Nitrate + Alumina			Temperature	Mass	cycle 1	cycle 2	cycle 3	cycle 1->2	cycle 2->3
Run Number	Method	Date	C	mg	J/gK	J/gK	J/gK	%	%
7	ASTM	8/12/2010	450	6.48	2.022	2.086	2.095	3.17%	0.43%
8	ASTM	8/13/2010	450	7.10	1.872	1.915	1.922	2.30%	0.37%
9	ASTM	11/11/2010	450	17.47	1.807	1.863	1.742	3.10%	-6.49%
10	MDSC	11/5/2010	450	9.86	1.561	1.548	1.260	0.83%	-18.60%
11	MDSC	9/18/2010	450	7.94	1.799	1.808	1.813	0.50%	0.28%
12	MDSC	10/1/2010	450	10.45	1.733	1.725	1.756	0.46%	1.80%
13	MDSC	10/2/2010	450	8.56	1.888	1.901	1.931	0.69%	1.58%
14	MDSC	10/3/2010	450	8.20	1.824	1.845	1.856	1.15%	0.60%

The nitrate + alumina remained stable up to 450C in almost all the sample tests, as can be seen in Table 8. The majority of the tests showed cycle to cycle variations below the DSC uncertainty. The exceptions are runs 9 and 10. These runs showed significant variations between cycles. Run 9 is strange in that is shows an increase then a decrease. The total percentage shift between cycle 1 and cycle 3 is small, but it is unknown why there would be an increase then a decrease. The other aberrant sample, run 10, showed a significant decrease in the cycle 2 to 3 comparison. The reasons for this are unclear, but as it only happened in one cycle of one sample, it seems to be an outlier. Additionally, that single sample showed a significantly lower specific heat than any other nitrate + alumina sample, so it seems that the sample itself was different from the other tested samples.

4.4.3 Nitrate + Silica Stability Results

Table 9: Nitrate + silica stability analysis. Above 400 C, the nitrate + silica was unstable.

Nitrate + Silica			Temperature	Mass	cycle 1	cycle 2	cycle 3	cycle 1->2	cycle 2->3
Run Number	Method	Date	C	mg	J/gK	J/gK	J/gK	%	%
15	ASTM	7/30/2010	350	5.18	1.706	1.842	1.876	7.97%	1.85%
16	ASTM	8/2/2010	400	9.77	1.943	1.999	2.002	2.88%	0.15%
17	ASTM	8/20/2010	450	10.44	1.824	1.737	1.727	-4.77%	-0.58%
18	MDSC	11/1/2010	450	7.26	1.359	1.190	1.079	-12.44%	-9.33%
19	MDSC	11/1/2010	425	9.41	1.720	1.668	1.599	-3.02%	-4.14%
20	MDSC	11/3/2010	400	9.77	1.731	1.728	1.727	-0.17%	-0.06%
21	MDSC	9/20/2010	400	9.77	1.825	1.849	1.854	1.32%	0.27%
22	MDSC	9/29/2010	400	10.23	1.688	1.721	1.743	1.95%	1.28%
23	MDSC	9/30/2010	400	12.99	1.806	1.825	1.839	1.05%	0.77%

A significant observed secondary property of the nitrate + SiO_2 1% mixture was a temperature-dependent specific heat reduction during the runs. Above 400C, the composite material showed a discernable decline in observed specific heat. Several runs were used to determine this temperature limit, as seen in Table 9. Figure 15-20 show the time and temperature based specific heat plots, to more clearly show the decay effect. The plots show the data from two separate runs of the same sample, one using the ASTM method, the other using the MDSC method. For example, Figure 15 and Figure 16 show tests of the same sample, with Figure 15 being the ASTM test and Figure 16 being the MDSC test. The ASTM test was run first, then the MDSC test was run on the same sample second. The time plots use the MDSC method, as the individual profile duration of the MDSC method is several times longer than the ASTM sample run. This difference in duration allows the MDSC run to more clearly show the property changes over time.

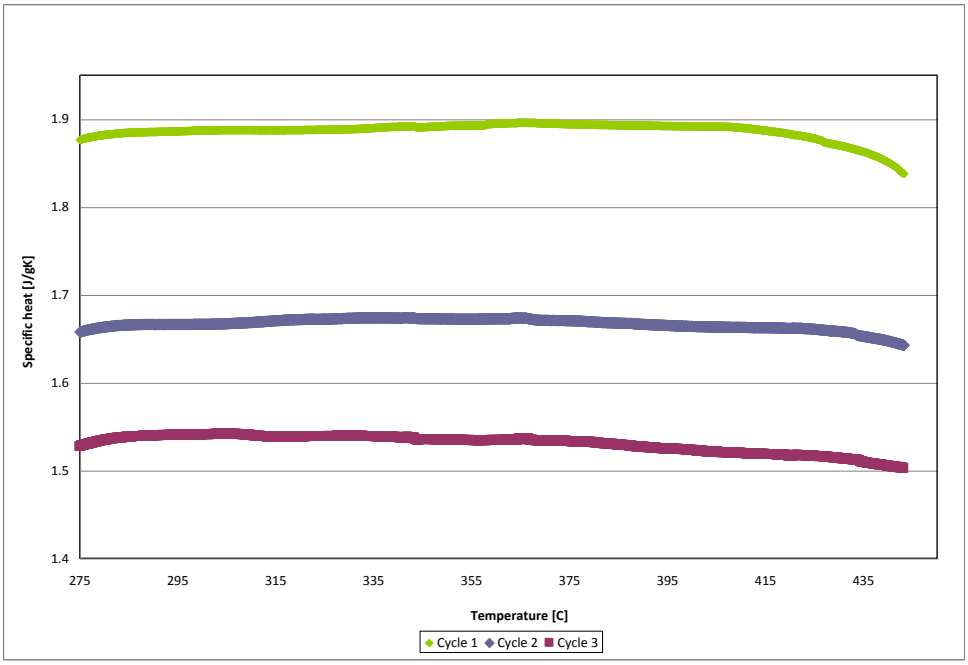

Figure 15: Specific heat of nitrate and silica 450 C maximum temperature run, showing the significant decrease in specific heat from cycle to cycle. Cycle 1 has the highest specific heat, followed by cycle 2 in the middle, and cycle 3 with the lowest.

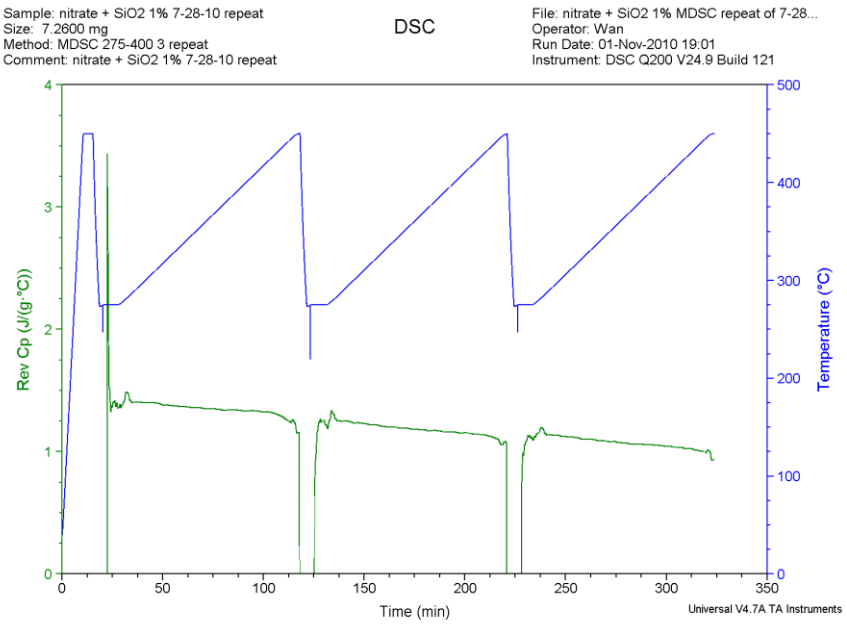

Figure 16: Second run of Figure 15 sample using MDSC, maximum temperature of 450 C. The specific heat decreases over time, even when the temperature is below 450 C. The upper line is the temperature, and the lower line is the specific heat.

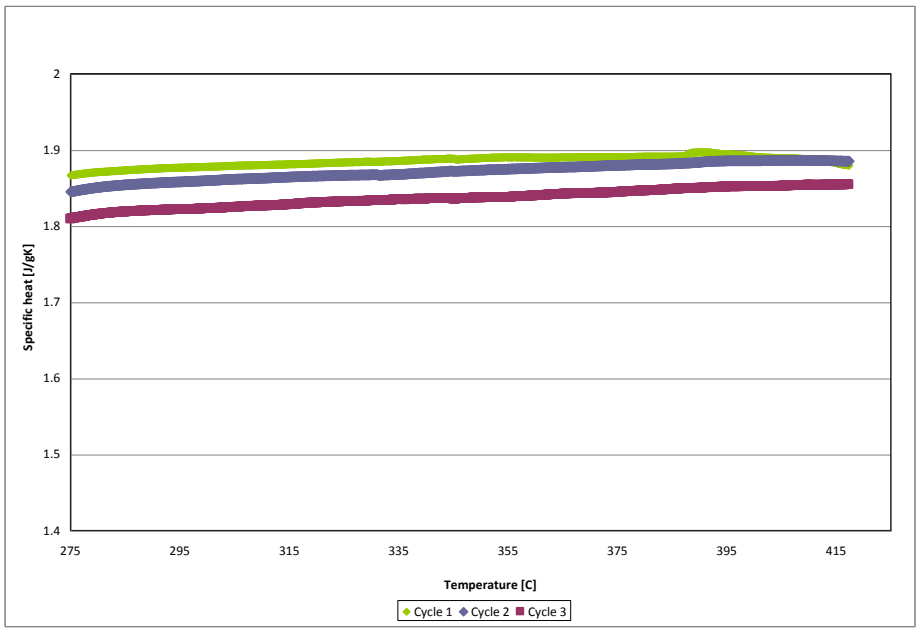

Figure 17: Nitrate and silica 425C maximum temperature run, showing a smaller decrease in specific heat when compared to the results shown in Figure 15. Cycle 1 has the highest specific heat, followed by cycle 2 with slightly lower specific heat, and cycle 3 has the lowest.

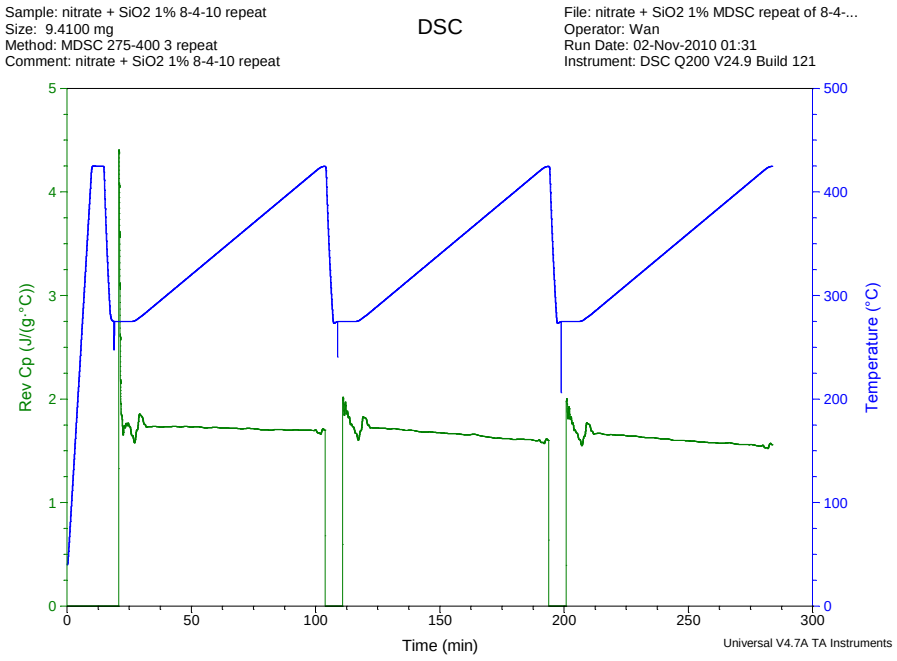

Figure 18: Nitrate + silica 425 C maximum temperature run using MDSC, second run of the sample from Figure 17. The specific heat decreases over time, even when the temperature is below 425 C. The upper line is the temperature, and the lower line is the specific heat.

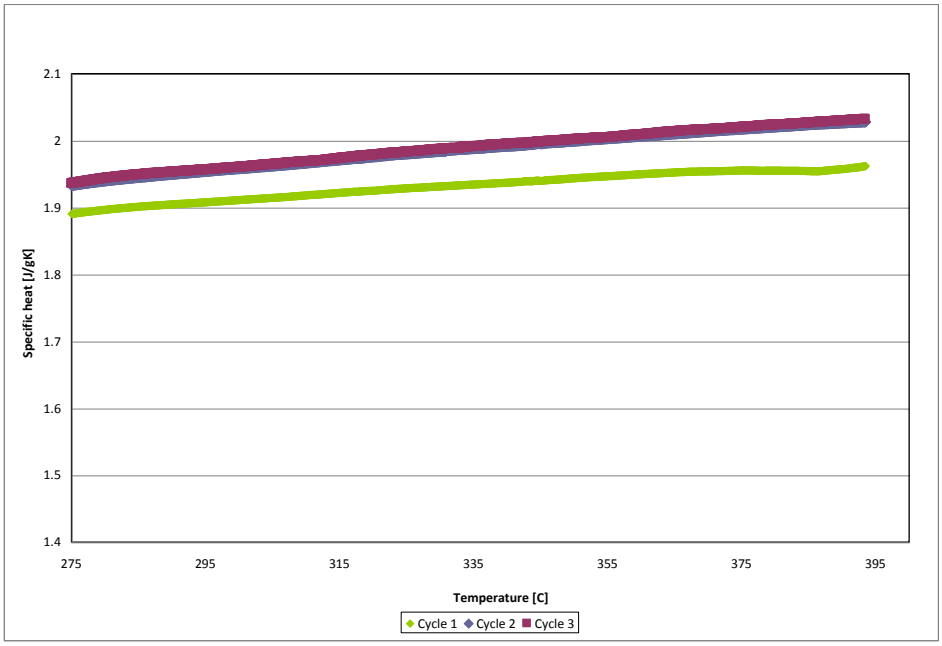

Figure 19: Specific heat of nitrate + silica, maximum run temperature of 400C. Cycle 1 has the lowest specific heat, but cycle 2 and cycle 3 have nearly the same specific heat, which indicates a stable specific heat.

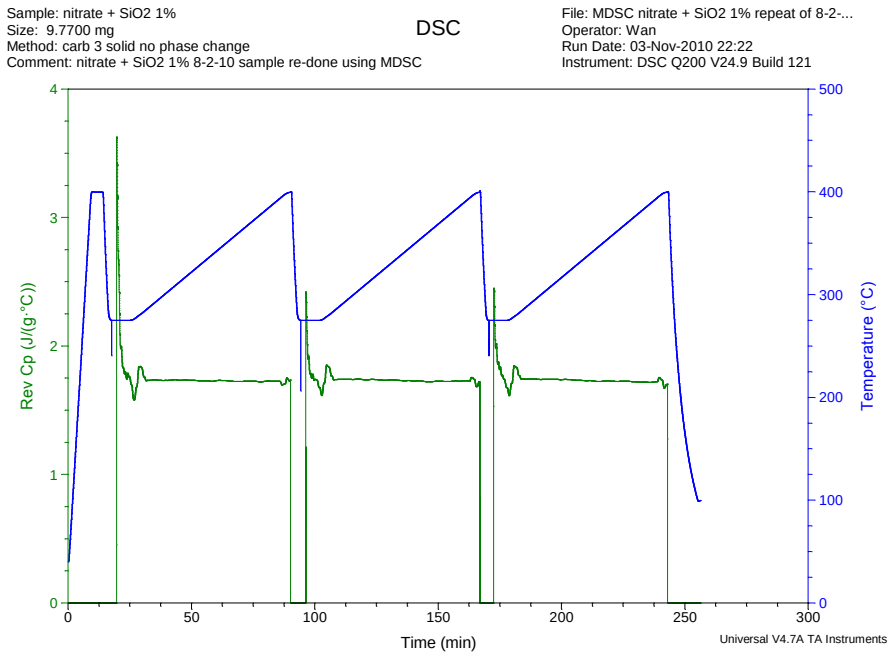

Figure 20: Specific heat of nitrate + silica 400 C maximum temperature run using MDSC, second run of the sample from Figure 19. The specific heat is stable over time, even when at the maximum temperature of the test. The upper line is the temperature, and the lower line is the specific heat.

As can be seen in Figures 15-20, the specific heat changes only when the run temperature goes above 400C. For all runs, the maximum temperature given was the maximum temperature of all ramp segments in the thermal profile. The change rate also seems to be related to the maximum run temperature, as the change in specific heat is larger at a 450C maximum run temperature than at a 425C maximum temperature. The 400C maximum temperature showed no significant change over time. For this reason, the rest of the silica composite runs (as listed in Table 9) were limited to 400C. In comparison, the nitrate + Al_2O_3 had no such observed behavior and was stable up to 450C in the runs. The observed maximum temperature of 400 C is a major limitation of this composite material, as current trough systems operate between 300 C to 400 C. Future improvements may increase the operational temperature range of the trough systems, which would prevent the silica composite from functioning properly in a TES system for a trough CSP plant. Additionally, the current tower systems operate at temperatures up to 600 C, much higher than the 400 C maximum temperature of the stable silica composite. Therefore, the nitrate and silica composite, while useful in current systems, may have limited future utility due to the observed stability issues.

5. FINDINGS

The results answered the questions presented in the introduction and met all the objectives. Based on the results, several findings can be drawn:

- The addition of the alumina and silica nanoparticles to the nitrate using the given method caused an increase in the specific heat compared to the plain nitrate over the entire temperature range of interest.
- The addition of the nanoparticles using the given method did not significantly alter the heat of fusion of the nitrate mixture.
- The combination of the nitrate and silica using the given method in an aluminum container undergoes some change when raised to a temperature above 400C, causing the specific heat to drop over time.
- The nitrate and alumina composite gave stable specific heat results up to 450C.
- The ASTM and MDSC methods were determined to be functionally equivalent, based on the results generated by each method.

Each of these findings can be directly linked with specific results from the results section. These findings are used to generate conclusions, presented next.

6. CONCLUSIONS

Based on the findings, several conclusions can be drawn:

- The addition of ceramic nanoparticles seems to enhance the specific heat of the nitrate eutectic, even at low mass percentages using the presented manufacturing method.
- The specific heat modification remained stable for both several phase changes and several hours in the liquid state.
- The heat of fusion of the nitrate does not seem to be altered by the addition of nanoparticles.
- Nanoparticle augmentation of the thermophysical properties of the nitrate for use in a TES system will work.
- The composite can be implemented into existing system designs to improve the performance of such systems without additional equipment or sub-systems.

Using these conclusions, it can be seen that the nitrate composite can be of benefit in existing and future TES systems, implemented in a CSP plant or other power generation facility.

NOMENCLATURE

ASTM	American Society for Testing and Materials
B(T)	Baseline heat flow value
C	Degrees Celsius
C_p	Specific heat capacity
C_{Ps}	Sample specific heat capacity
C_{Pr}	Standard/reference specific heat capacity
CSP	Concentrating Solar Power
$D_s(T)$	Corrected standard/reference heat flow value
$D_r(T)$	Corrected sample heat flow value
DOE	Department of Energy
DSC	Differential Scanning Calorimetry
g	Gram
H_f	Heat of fusion
hr	Hour
HTF	Heat Transfer Fluid
J	Joule
K	Kelvin
kg	Kilogram
MWh_t	Thermal megawatt-hour
MWh_e	Electrical megawatt-hour
m	Meter

MDSC	Modulating Differential Scanning Calorimetry
mg	Milligram
mL	Milliliter
M_R	Standard/reference mass
M_S	Sample mass
NREL	National Renewable Energy Laboratory
Q	Thermal energy absorbed
R(T)	Standard/reference heat flow value
s	Second
S(T)	Sample heat flow value
TA	Thermal Analysis
TES	Thermal Energy Storage
TGDSC	Thermogravimetric DSC
ΔT	Change in temperature (T_H-T_L)

REFERENCES

1.) Coastal Chemical L.L.C. Hitec solar salt coastal chemical specification sheet. Coastal Chemical L.L.C., Houston TX. 2010.

2.) Janz GJ, Allen CB, Bansal NP, Murphy RM, Tomkins RPT. Physical properties data compilations relevant to energy storage: molten salts: data on single and multi-component salt systems. Rensselaer Polytechnic Institute, Troy, New York, April 1979; 396-411.

3.) Janz GJ, Allen CB, Murphy RM, Tomkins RPT. Physical properties data compilations relevant to energy storage I: molten salts eutectic data. *NSRDS-NBS-61;* US Government Printing Office, Washington DC, 1978.

4.) Peng Q, Wei X, Ding J, Yang J, Yang X. High-temperature thermal stability of molten salt materials. *International Journal of Energy Research*, 2008; **32**: 1164-1174.

5.) Eastman JA, Choi SUS, Li S, Thompson LJ Lee S. Enhanced thermal conductivity through the development of nanofluids. *Presented at the Materials Research Society 1996 Fall Meeting*, Boston MA, Dec. 2-6 1996.

6.) Eastman JA, Choi SUS, Li S, Thompson LJ, Yu W. Anomalously increased effective thermal conductivities of ethylene glycol-based nanofluids containing copper nanoparticles. *Applied Physics Letters*, 2001; **78**(6): 718-720.

7.) Wang X, Mujumdar A. Heat transfer characteristics of nanofluids: a review. *International Journal of Thermal Sciences,* 2007; **46:** 1-19.

8.) Wang B, Zhou L, Peng X. Surface and size effects on the specific heat capacity of nanoparticles. *International Journal of Thermophysics* 2006; **27**(1): 139-151.

9.) Zhou L, Wang B, Peng X, Du X, Yang Y. On the specific heat capacity of CuO nanofluid. *Advancements in Mechanical Engineering* 2009; Hindawi Publishing Corporation.

10.) Zhou S, Ni R. Measurement of the specific heat capacity of water-based Al_2O_3 nanofluid. *Applied Physics Letters*, 2008; **92**.

11.) Sundar L, Sharma KV, Ramanathan S. Experimental investigation of heat transfer enhancements with Al_2O_3 nanofluid and twisted tape insert in a circular tube. *International Journal of Nanotechnology and Applications,* 2007; **1** (2): 21-28.

12.) Likhachev VN, Astakhova T, Vinogradov GA, Alymov MI. Anomalous heat capacity of nanoparticles. *Russian Journal of Physical Chemistry B,* 2007; **1**(1): 89-93.

13.) Nelson IC, Banerjee D, and Rengasamy P. Flow loop experiments using polyalphaolefin nanofluids. *AIAA Journal of Thermophysics and Heat Transfer*, 2009; **23(**4):752-761.

14.) Shin D, and Banerjee D. Effects of silica nanoparticles on enhancing the specific heat capacity of carbonate salt eutectic (work in progress). *International Journal of Structural Change in Solids – Mechanics and Applications*, 2010 **2(**2):25-31.

15.) Malik. Evaluation of composite alumina nanoparticle and nitrate eutectic materials for use in concentrating solar power plants. Thesis. Texas A&M, 2010.

16.) Standard test method for determining specific heat capacity by differential scanning calorimetry, ASTM 1269E-05, *ASTM International*, 2009.

17.) Carling RW, Kramer CM, Bradshaw RW, Nissen DA, Goods SH, *et al*. Molten salt technology development status report. Report. *SAND80-8052*. Sandia National Laboratories, Livermore, 1981.

18.) Reddy RG, Zhang Z, Arenas MF, Blake DM. Thermal stability and corrosive evaluations of ionic liquids as thermal storage media. *High Temperature Materials and Processes*, 2003; **22**(2):87-94.

19.) Pacheco JE, Showalter SK, Kolb WJ. Development of a molten-salt thermocline thermal storage system for parabolic trough plants. *Journal of Solar Energy Engineering*, 2002; **124**:153-159.

20.) Moen L, Blake DM, Rudnicki DL, Hale MJ. Advanced thermal storage fluids for solar parabolic trough systems. *Transactions of the ASME*, 2003; **125**:112-116.

21.) Feng Y, Gui C, Chen J, Hu X. Thermal physical properties of bulk materials from ZrO2 nanoparticles by sintering process. *Key Engineering Materials*, Trans Tech Publications, Switzerland, 2007; **358:**1481-1484

22.) Thomas, LC. MDSC applications, solutions to materials characterization problems. *Netsu Sokutei,* 1995; **22**(2): 85-87.

23.) Calkins RJ, Lauro GF, Fretz KW, Majors DN, Mehta DD, *et al*. Conceptual design selection and development of a latent-heat thermal energy storage subsystem for a saturated steam solar receiver and load. Report. *SAND81-8184*. Sandia National Laboratories, 1981.

24.) Seyler RJ. Evaluation of thermal stability, an overview. *Thermochimica Acta,* 1980; **41**:55-62.

25.) Kearny D, Herrmann U, Nava P, Kelly B, Mahoney R, *et al*. Assessment of a molten salt heat transfer fluid in a parabolic trough solar field. *Transactions of the ASME,* 2003; **125**:170-176.

26.) Thermal Analysis Q200 manual, TA Instruments, New Castle, DE 2010.

27.) Thermal Analysis Q200 Special Topics Guide, TA Instruments, New Castle, DE 2010.

28.) Standard Test Method for the Thermal Stability of Chemicals by Differential Scanning Calorimetry, ASTM E537-07, *ASTM International* 2010.

29.) Gao L, Li W, Wang J, Guo JK. Influence of some parameters on the synthesis of ZrO2 nanoparticles by heating of alcohol-aqueous salt solutions. *Journal of Nanoparticle Research 1*, 1999; **1**:349-352

APPENDIX A

INDIVIDUAL RUN SPECIFIC HEAT TRACES

All plots shown in this appendix were generated in the same manner as the plots shown in the Results section, meaning ASTM method runs were plotted after computations described in the Method section, while MDSC results are plots of the raw output of the DSC itself. This appendix is broken down into three parts, with each material type having a part. All runs from Table 3 are presented in ascending run order, using the run numbers given in Table 3.

Plain Nitrate Specific Heat Plots, Runs 1 to 6

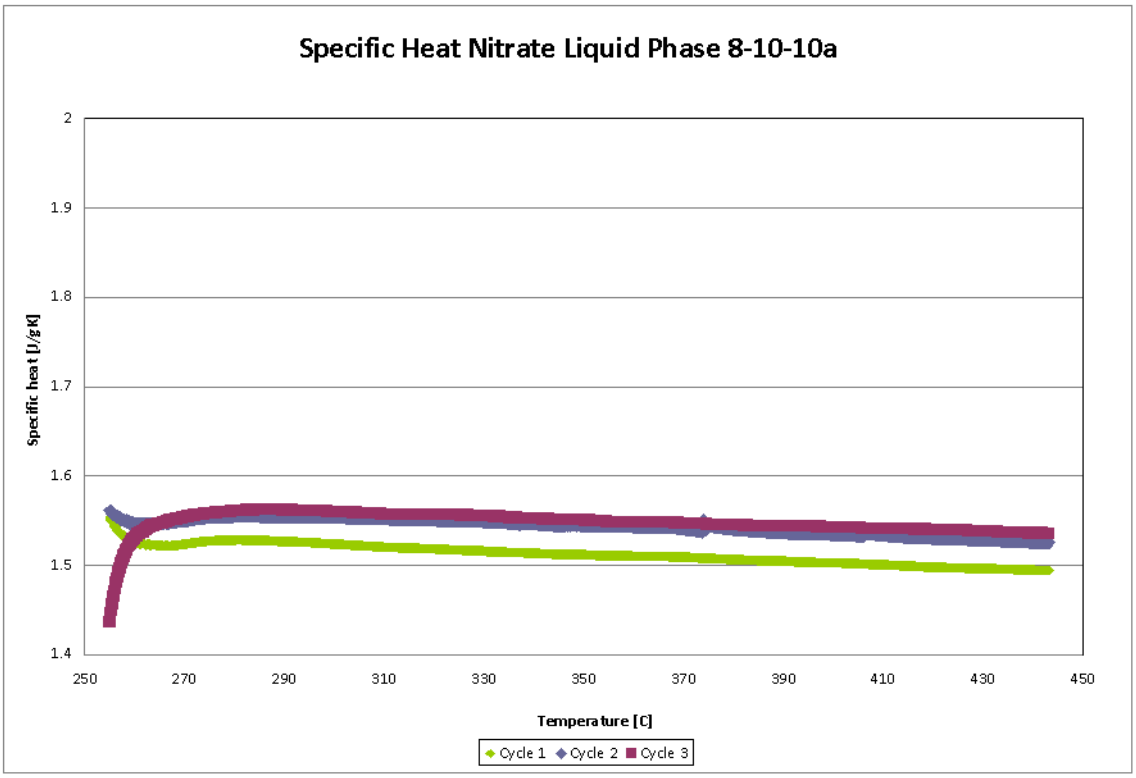

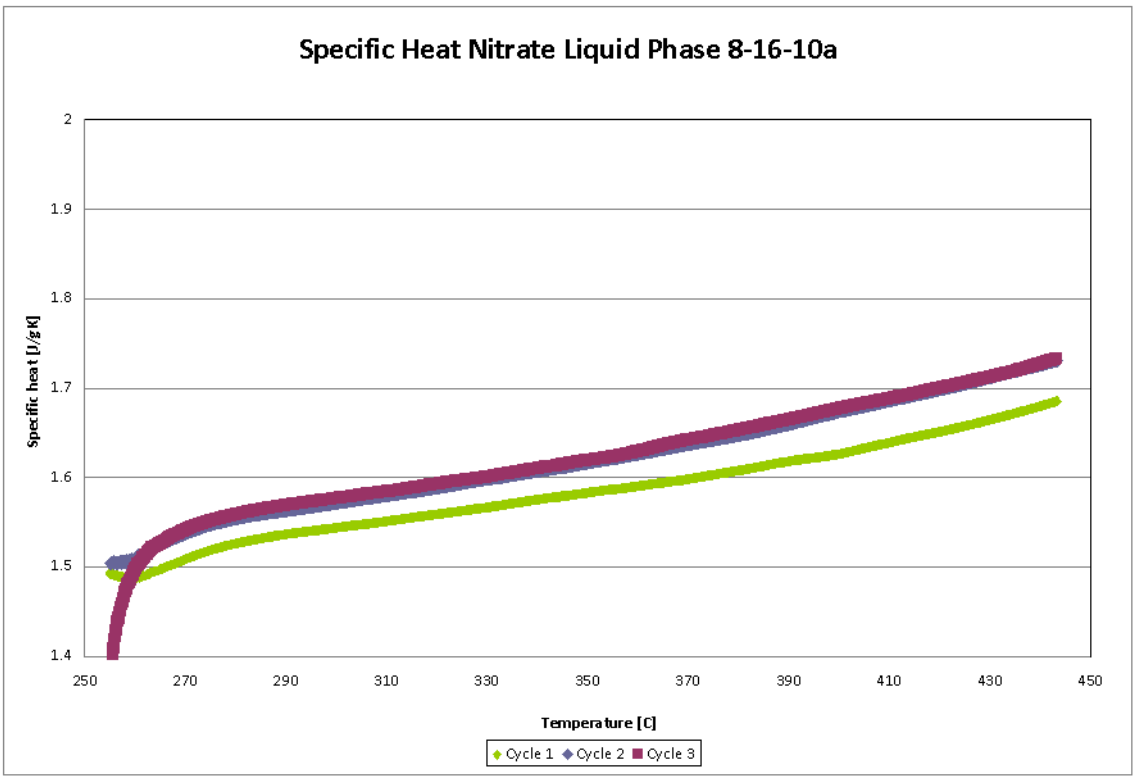
Specific Heat Nitrate Liquid Phase 8-16-10a
Specific heat [J/gK]
2
1.9
1.8
1.7
1.6
1.5
1.4
250
270
290
310
330
350
370
390
410
430
450
Temperature [C]
Cycle 1
Cycle 2
Cycle 3

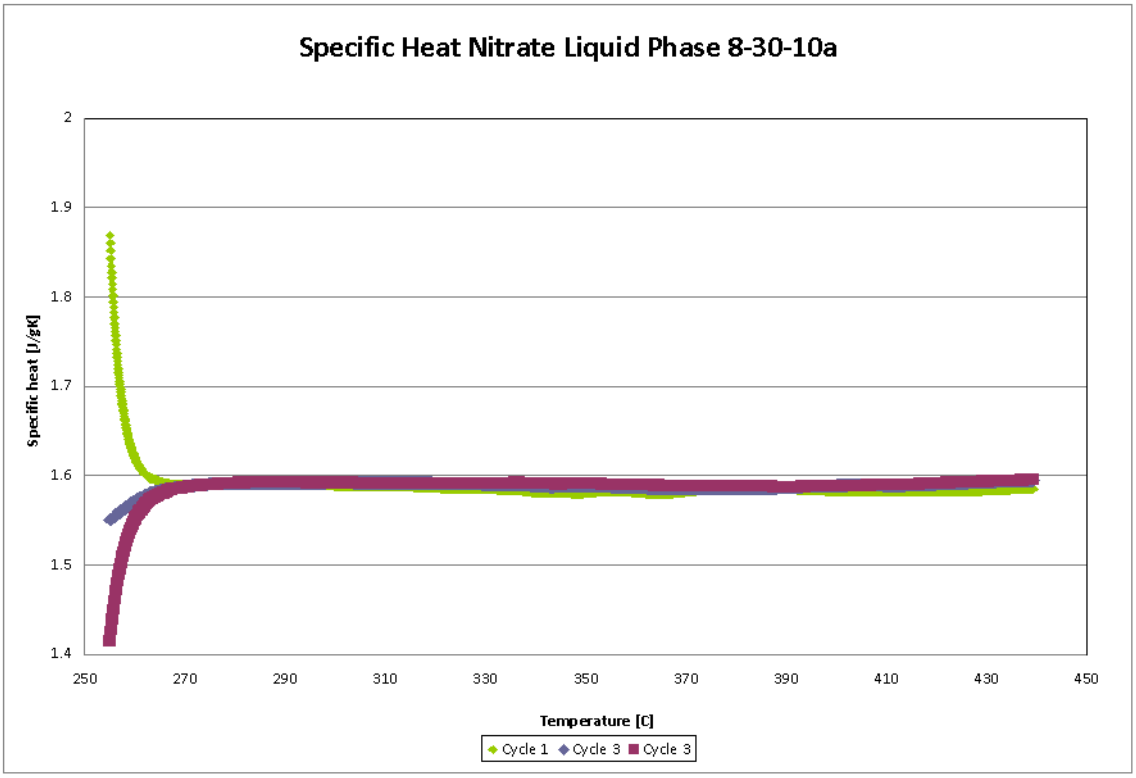
Specific Heat Nitrate Liquid Phase 8-30-10a
Specific heat [J/gK]
2
1.9
1.8
1.7
1.6
1.5
1.4
250
270
290
310
330
350
370
390
410
430
450
Temperature [C]
Cycle 1
Cycle 3
Cycle 3

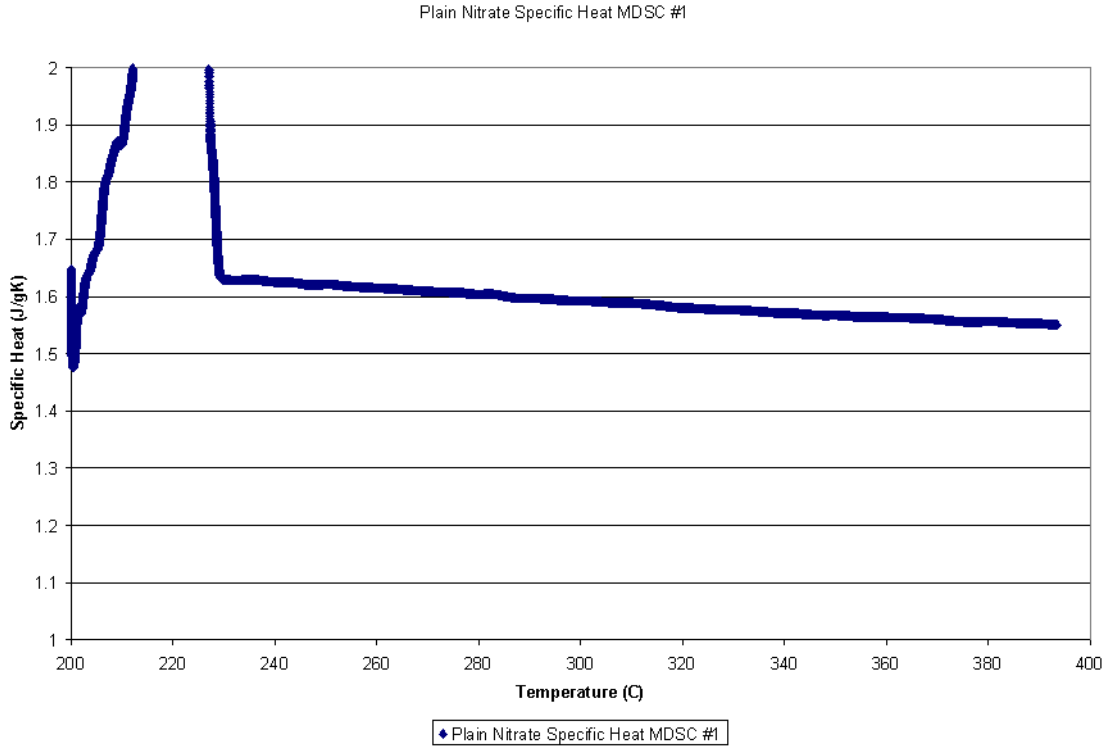
Plain Nitrate Specific Heat MDSC #1
Specific Heat (J/gK)
2
1.9
1.8
1.7
1.6
1.5
1.4
1.3
1.2
1.1
1
200
220
240
260
280
300
320
340
360
380
400
Temperature (C)
Plain Nitrate Specific Heat MDSC #1

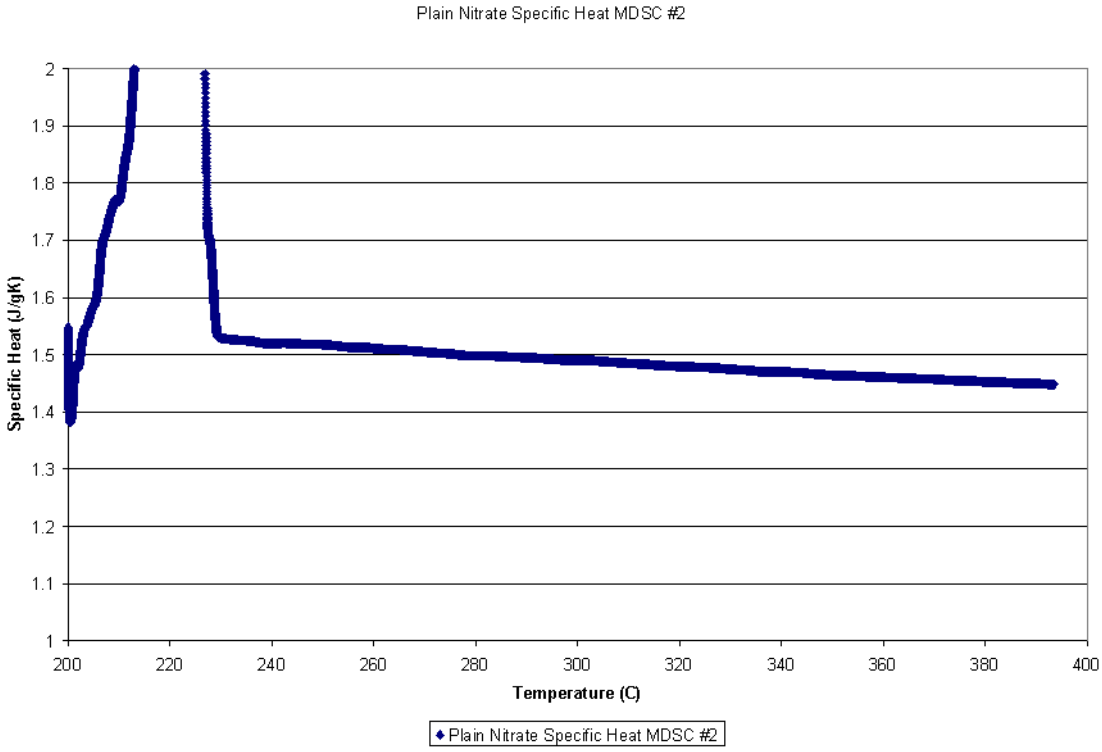
Plain Nitrate Specific Heat MDSC #2
Specific Heat (J/gK)
2
1.9
1.8
1.7
1.6
1.5
1.4
1.3
1.2
1.1
1
200
220
240
260
280
300
320
340
360
380
400
Temperature (C)
Plain Nitrate Specific Heat MDSC #2

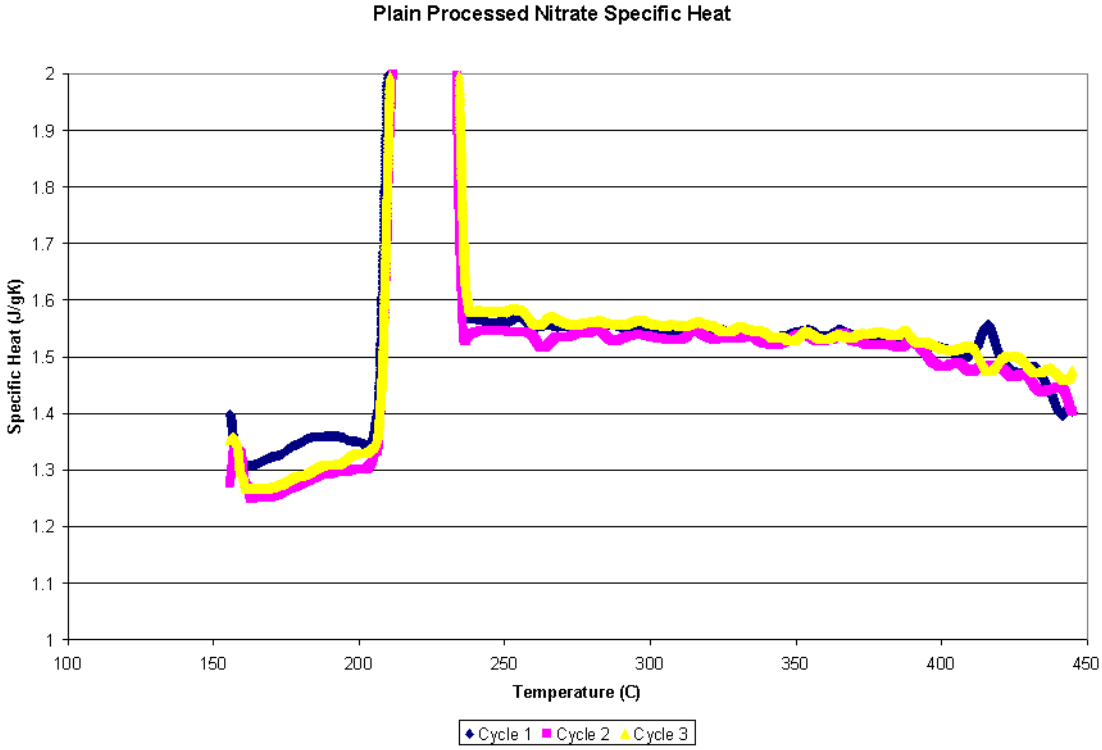
Plain Processed Nitrate Specific Heat
Specific Heat (J/gK)
2
1.9
1.8
1.7
1.6
1.5
1.4
1.3
1.2
1.1
1
100
150
200
250
300
350
400
450
Temperature (C)
Cycle 1
Cycle 2
Cycle 3

Nitrate and Alumina Plots, Runs 7-14

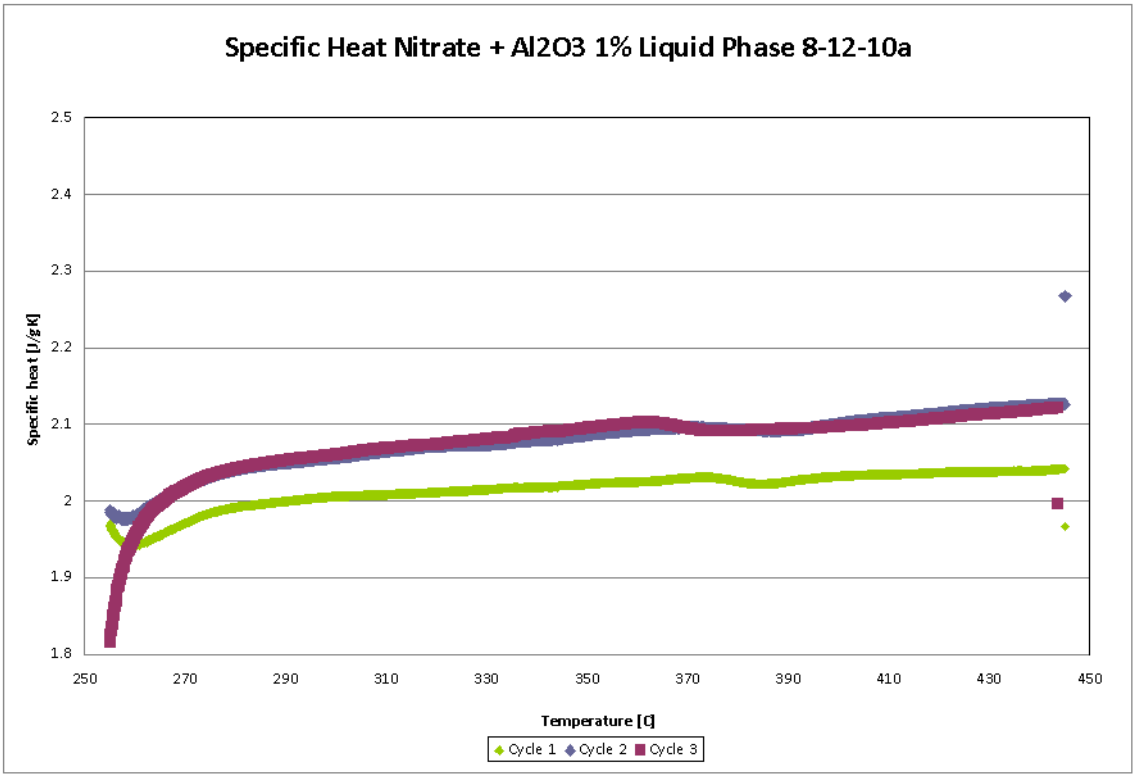

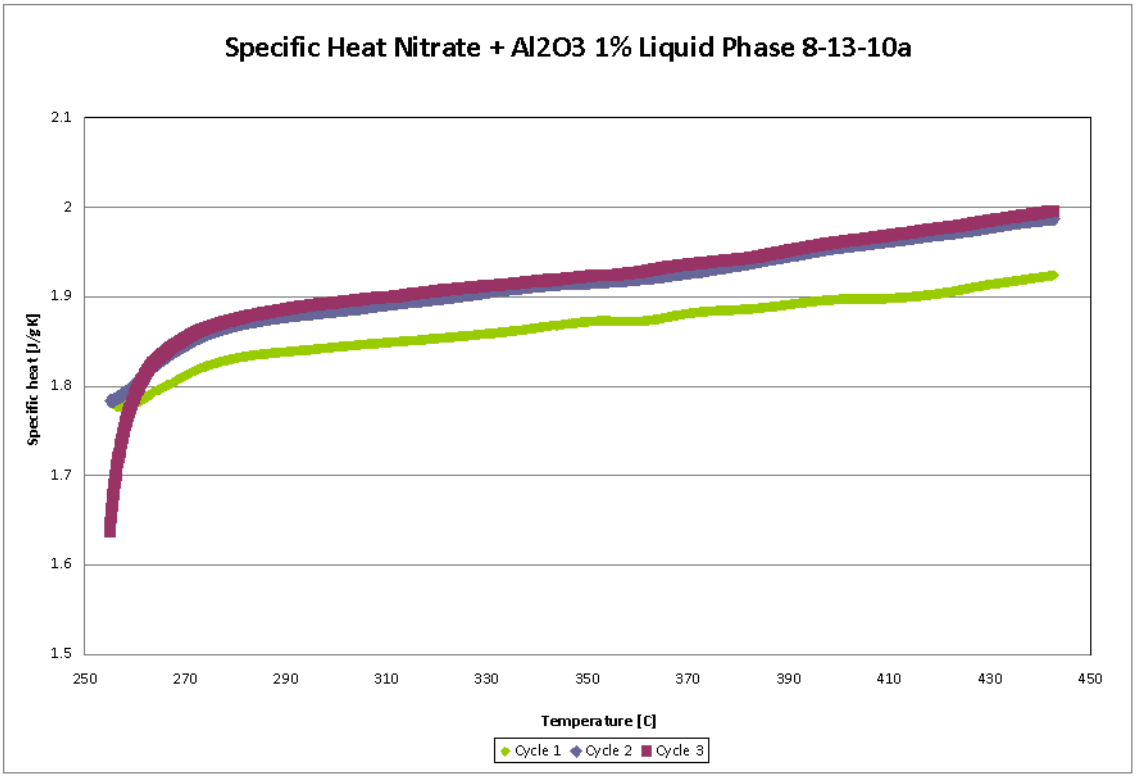
Specific Heat Nitrate + Al2O3 1% Liquid Phase 8-13-10a
Specific heat [J/gK]
2.1
2
1.9
1.8
1.7
1.6
1.5
250
270
290
310
330
350
370
390
410
430
450
Temperature [C]
Cycle 1
Cycle 2
Cycle 3

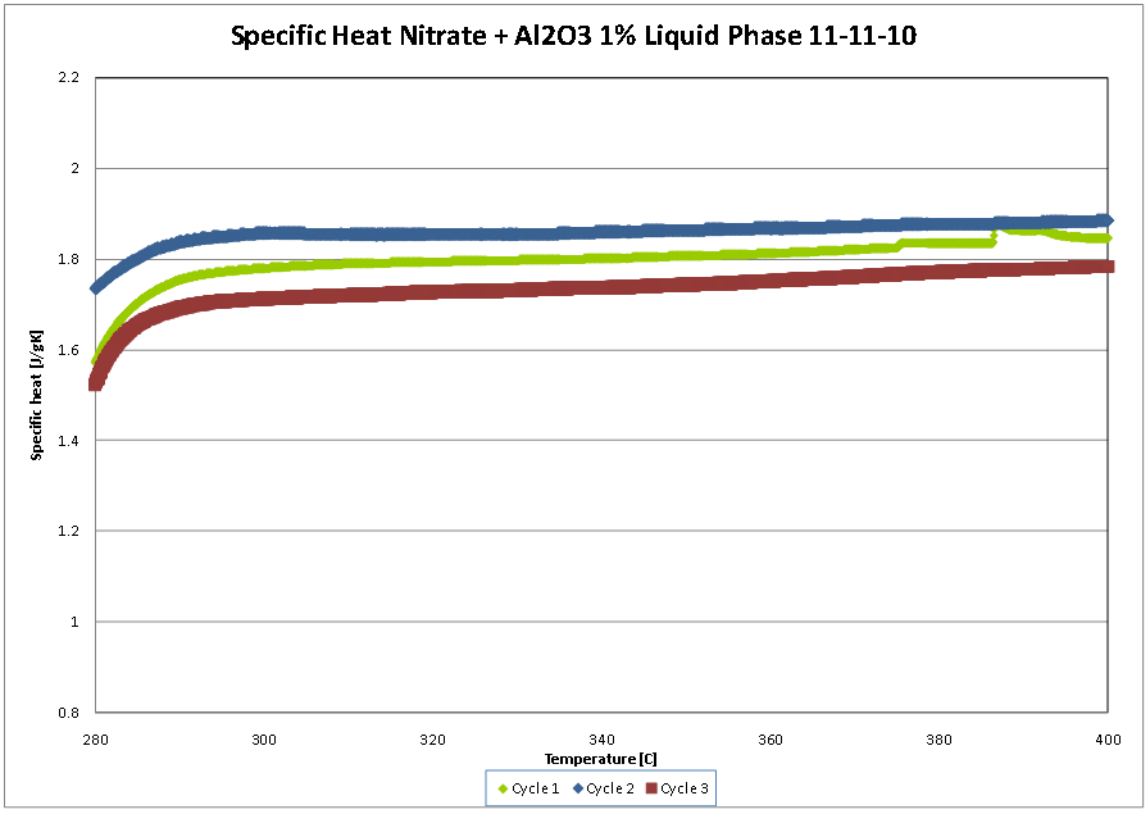
Specific Heat Nitrate + Al2O3 1% Liquid Phase 11-11-10
Specific heat [J/gK]
2.2
2
1.8
1.6
1.4
1.2
1
0.8
280
300
320
340
360
380
400
Temperature [C]
Cycle 1
Cycle 2
Cycle 3

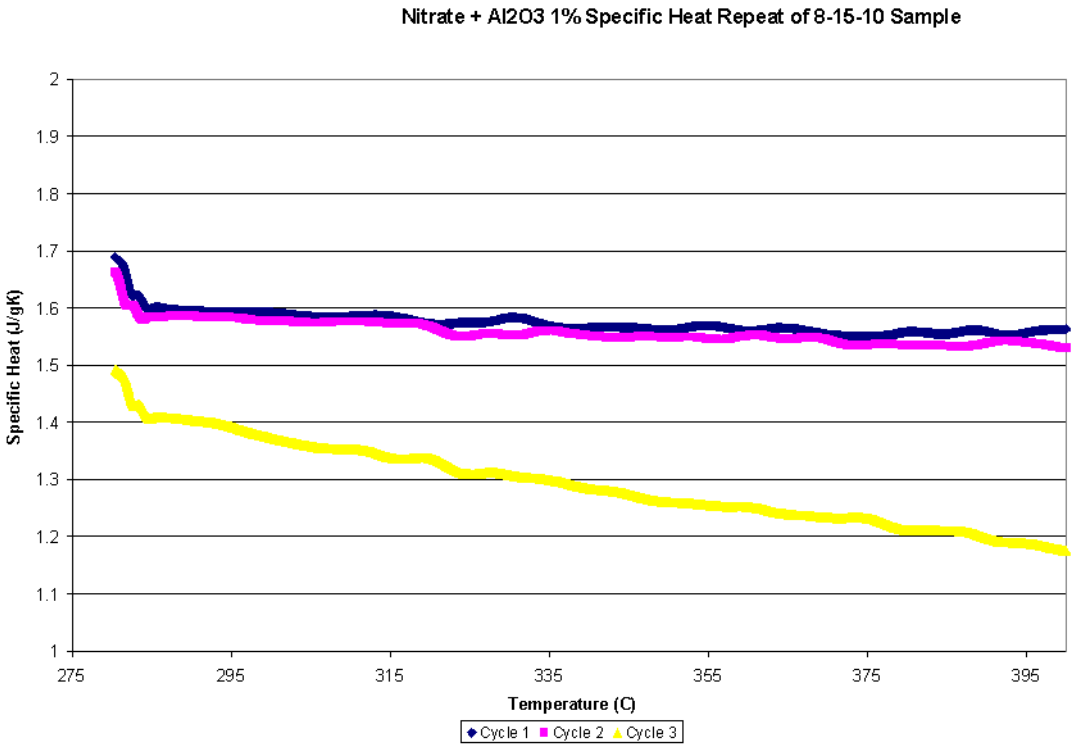
Nitrate + Al2O3 1% Specific Heat Repeat of 8-15-10 Sample
Specific Heat (J/gK)
2
1.9
1.8
1.7
1.6
1.5
1.4
1.3
1.2
1.1
1
275
295
315
335
355
375
395
Temperature (C)
Cycle 1
Cycle 2
Cycle 3

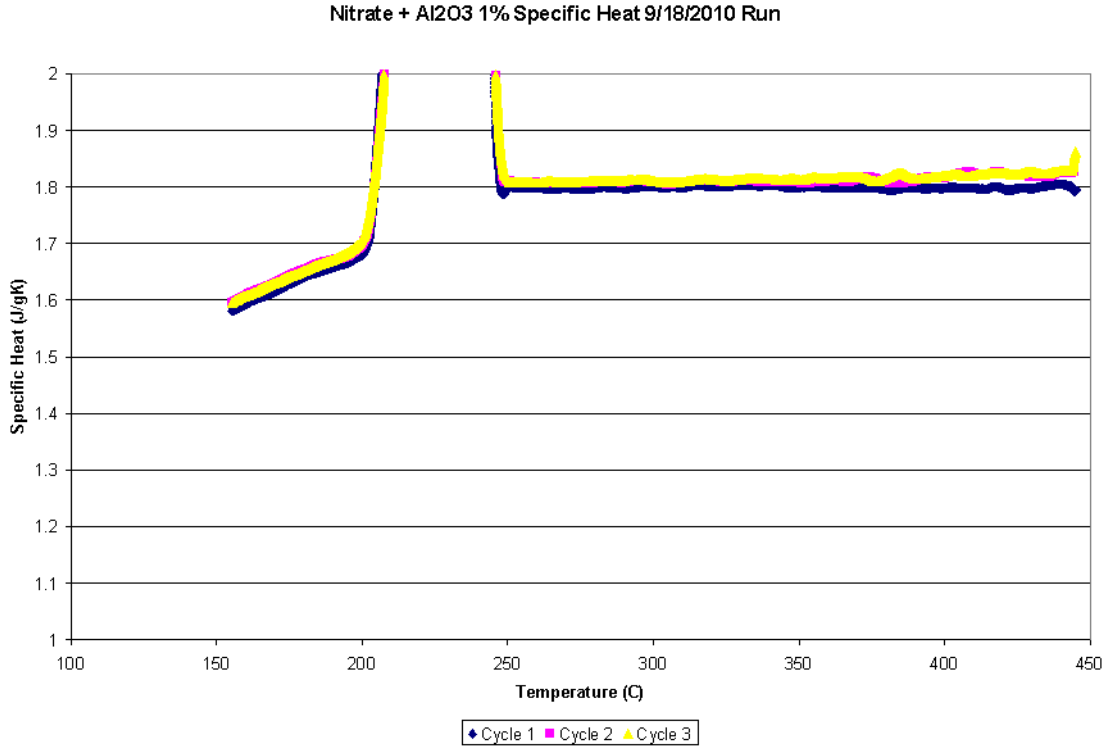
Nitrate + Al2O3 1% Specific Heat 9/18/2010 Run
Specific Heat (J/gK)
2
1.9
1.8
1.7
1.6
1.5
1.4
1.3
1.2
1.1
1
100
150
200
250
300
350
400
450
Temperature (C)
Cycle 1
Cycle 2
Cycle 3

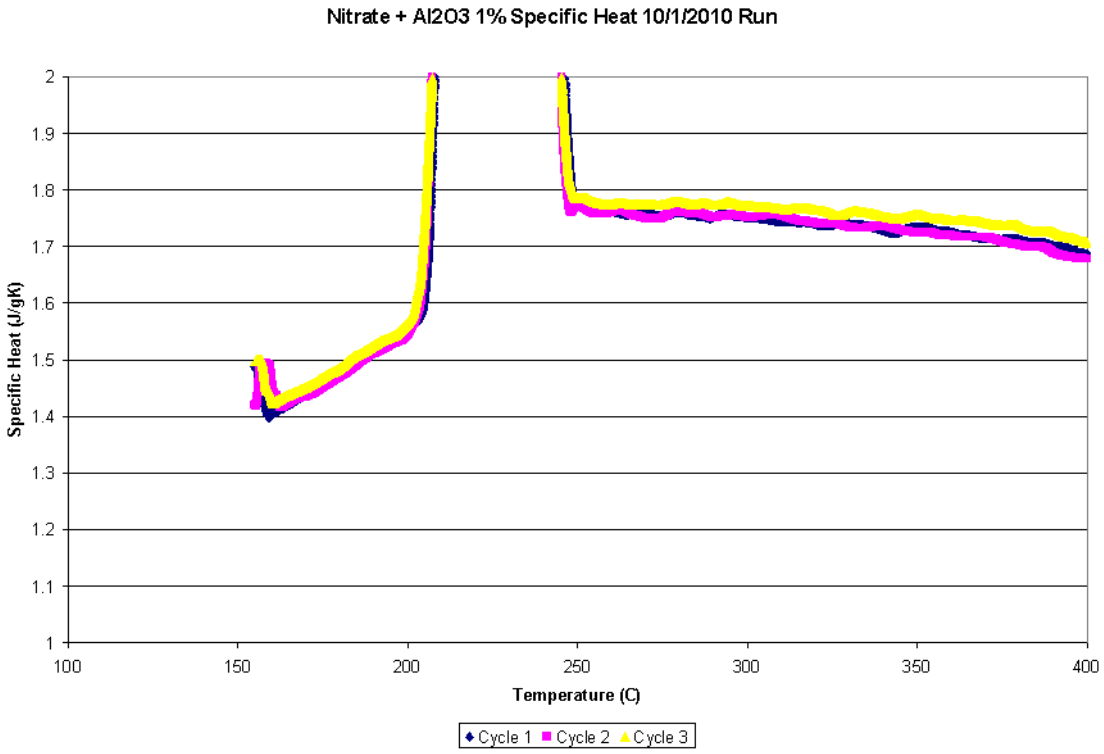
Nitrate + Al2O3 1% Specific Heat 10/1/2010 Run
Specific Heat (J/gK)
2
1.9
1.8
1.7
1.6
1.5
1.4
1.3
1.2
1.1
1
100
150
200
250
300
350
400
Temperature (C)
Cycle 1
Cycle 2
Cycle 3

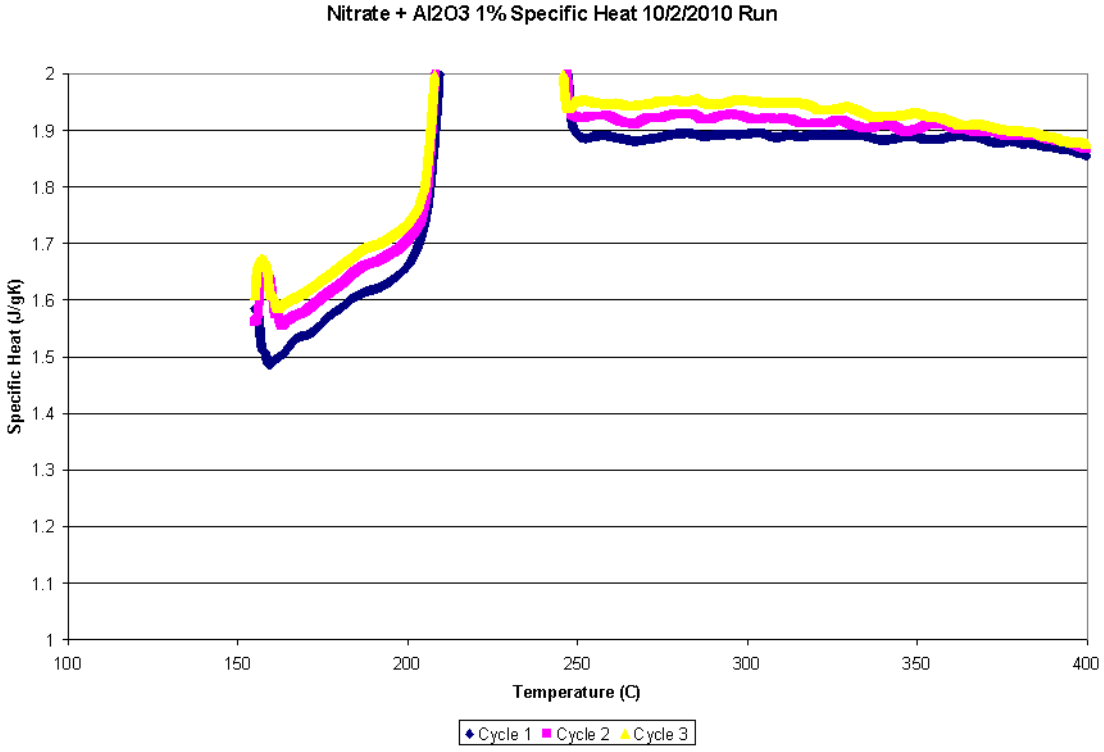
Nitrate + Al2O3 1% Specific Heat 10/2/2010 Run
Specific Heat (J/gK)
2
1.9
1.8
1.7
1.6
1.5
1.4
1.3
1.2
1.1
1
100
150
200
250
300
350
400
Temperature (C)
Cycle 1
Cycle 2
Cycle 3

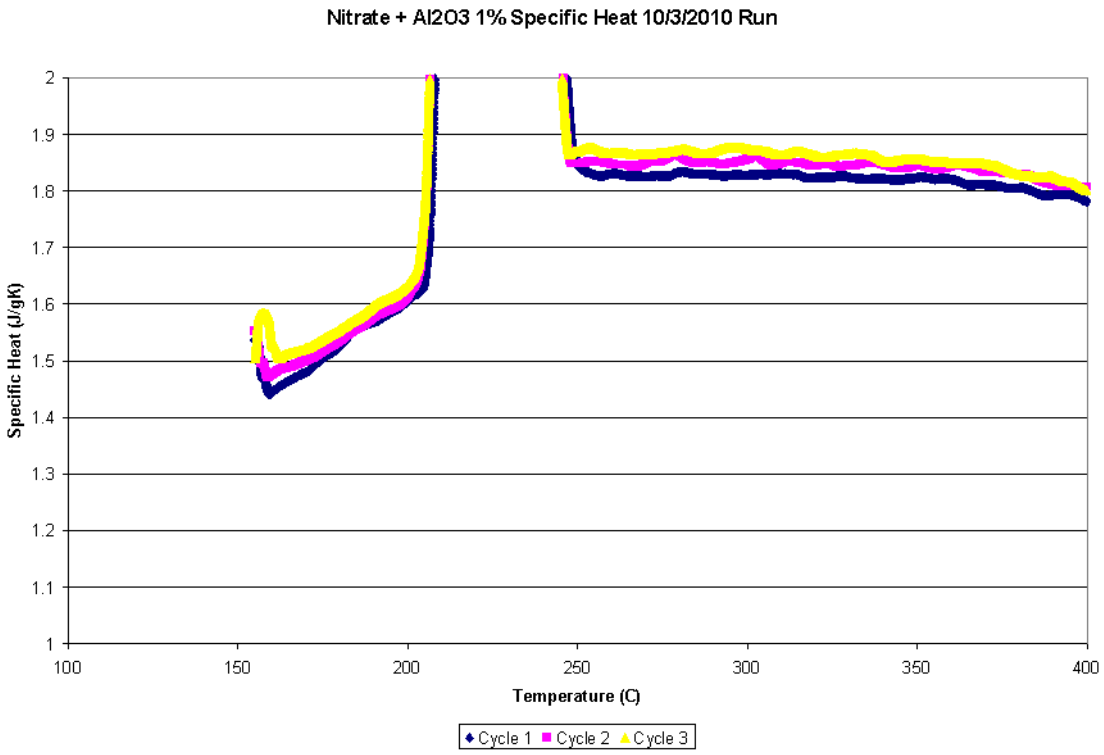
Nitrate + Al2O3 1% Specific Heat 10/3/2010 Run
Specific Heat (J/gK)
2
1.9
1.8
1.7
1.6
1.5
1.4
1.3
1.2
1.1
1
100
150
200
250
300
350
400
Temperature (C)
Cycle 1
Cycle 2
Cycle 3

Nitrate and Silica Plots, Runs 15-23

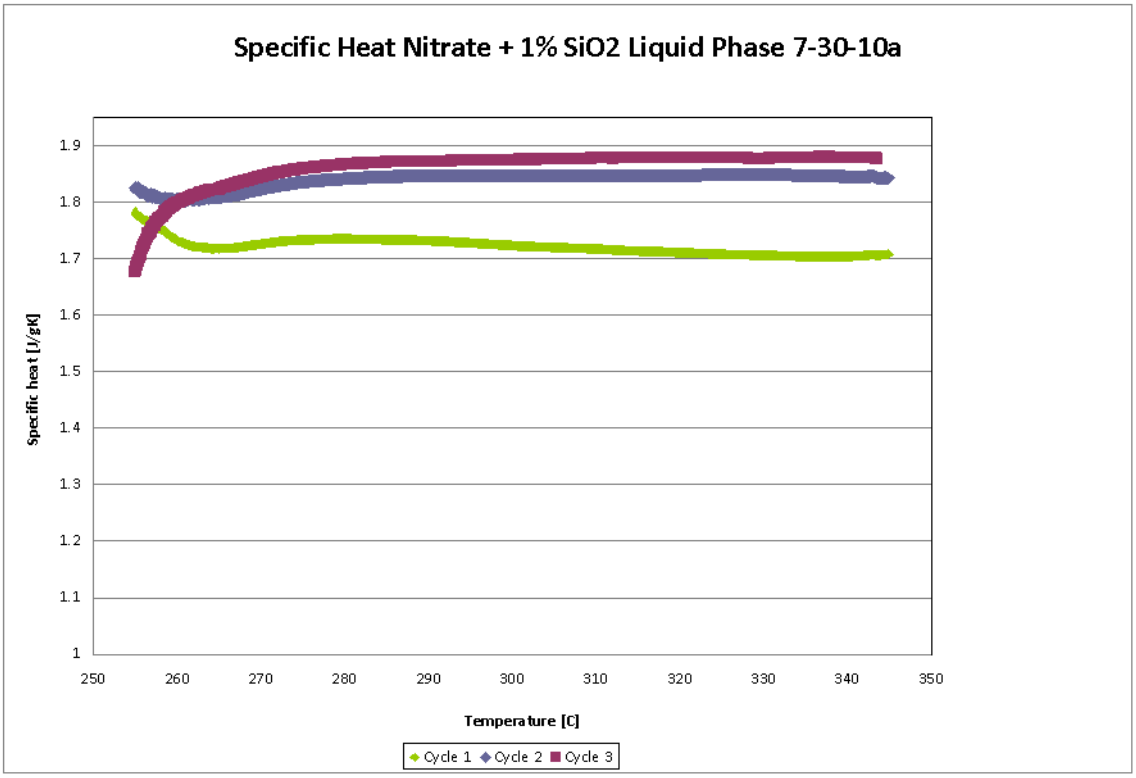

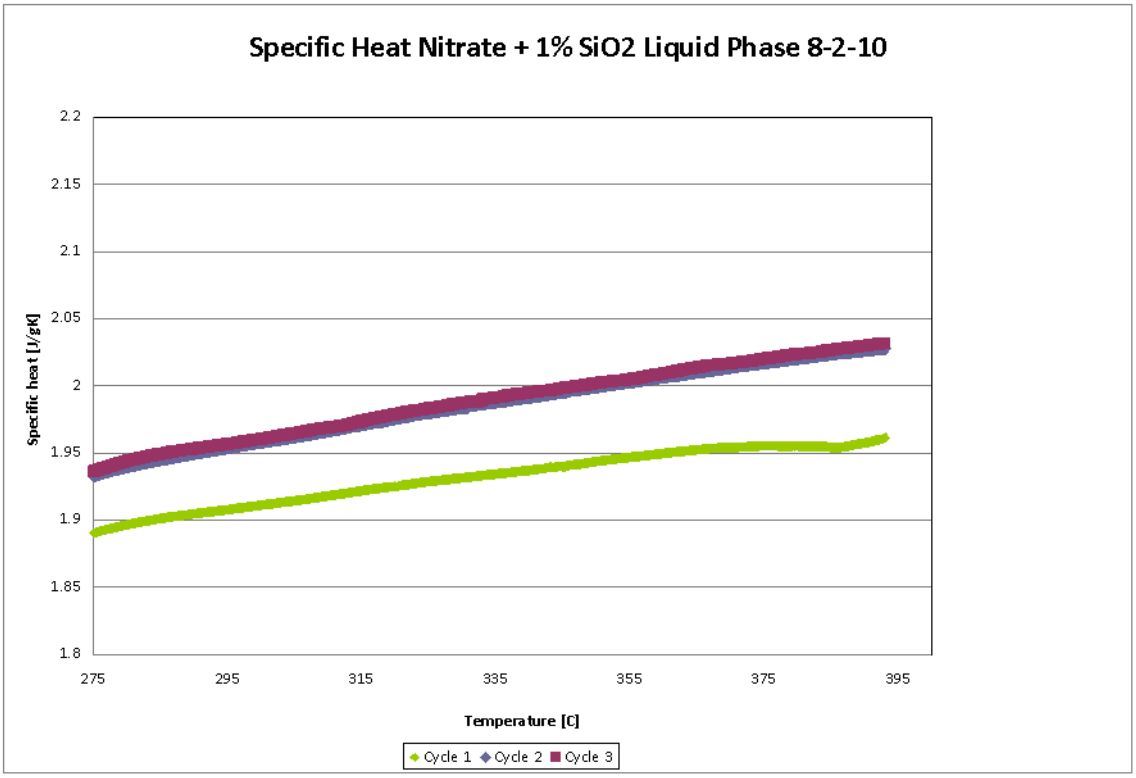
Specific Heat Nitrate + 1% SiO2 Liquid Phase 8-2-10
Specific heat [J/gK]
2.2
2.15
2.1
2.05
2
1.95
1.9
1.85
1.8
275
295
315
335
355
375
395
Temperature [C]
Cycle 1
Cycle 2
Cycle 3

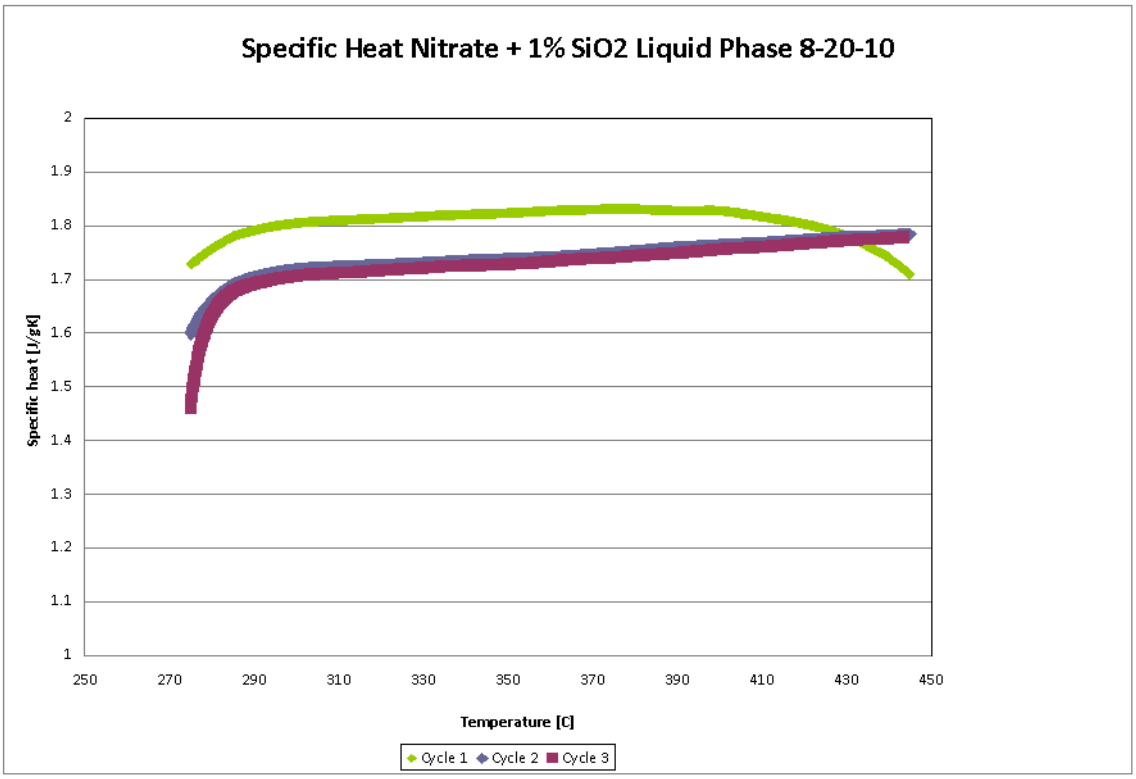
Specific Heat Nitrate + 1% SiO2 Liquid Phase 8-20-10
Specific heat [J/gK]
2
1.9
1.8
1.7
1.6
1.5
1.4
1.3
1.2
1.1
1
250
270
290
310
330
350
370
390
410
430
450
Temperature [C]
Cycle 1
Cycle 2
Cycle 3

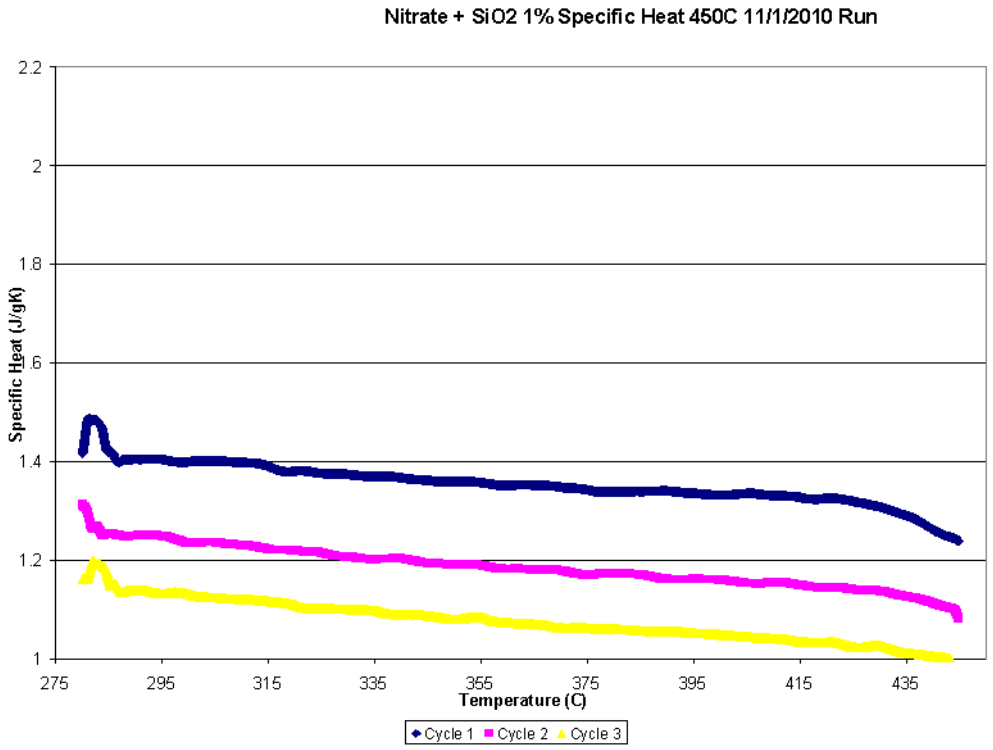
Nitrate + SiO2 1% Specific Heat 450C 11/1/2010 Run
Specific Heat (J/gK)
2.2
2
1.8
1.6
1.4
1.2
1
275
295
315
335
355
375
395
415
435
Temperature (C)
Cycle 1
Cycle 2
Cycle 3

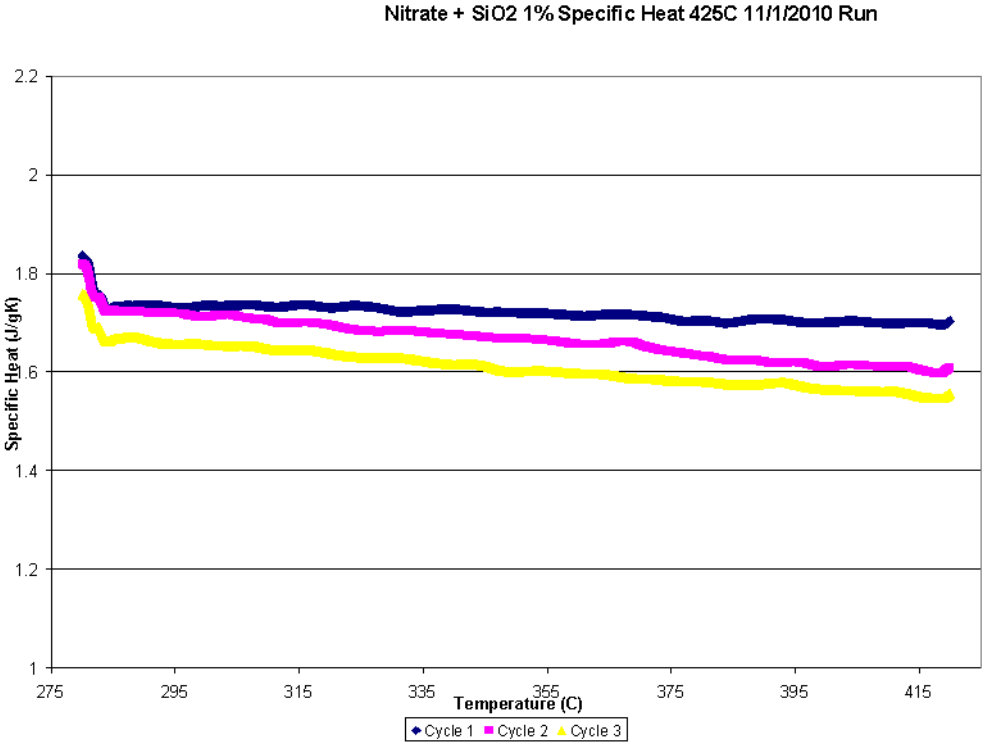
Nitrate + SiO2 1% Specific Heat 425C 11/1/2010 Run
Specific Heat (J/gK)
2.2
2
1.8
1.6
1.4
1.2
1
275
295
315
335
355
375
395
415
Temperature (C)
Cycle 1
Cycle 2
Cycle 3

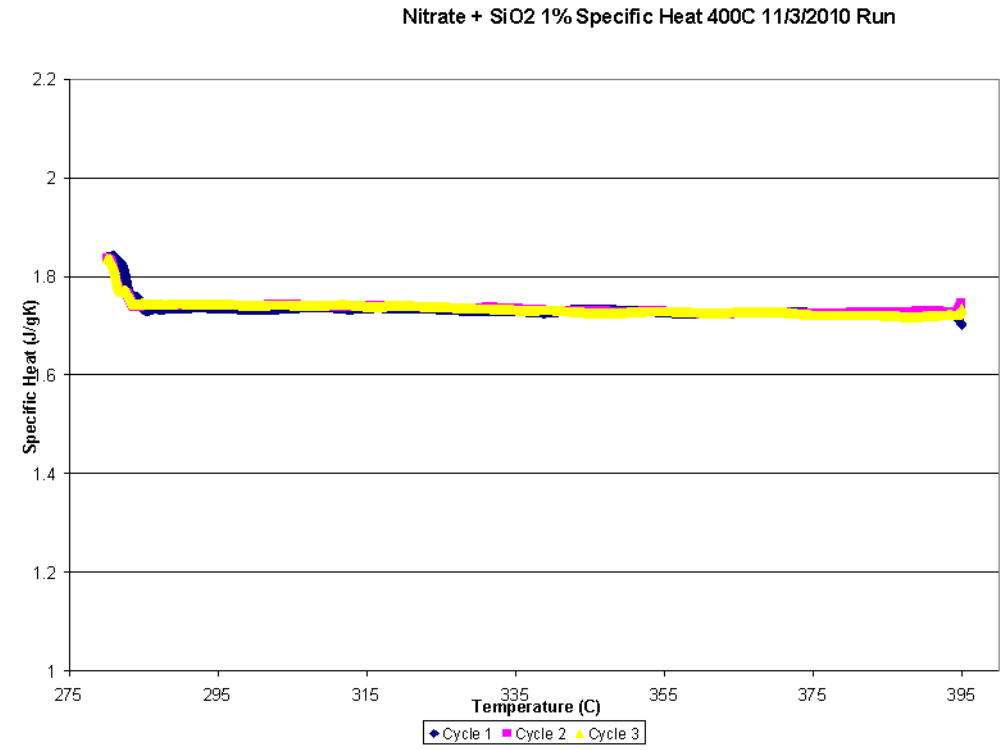
Nitrate + SiO2 1% Specific Heat 400C 11/3/2010 Run
Specific Heat (J/gK)
2.2
2
1.8
1.6
1.4
1.2
1
275
295
315
335
355
375
395
Temperature (C)
Cycle 1
Cycle 2
Cycle 3

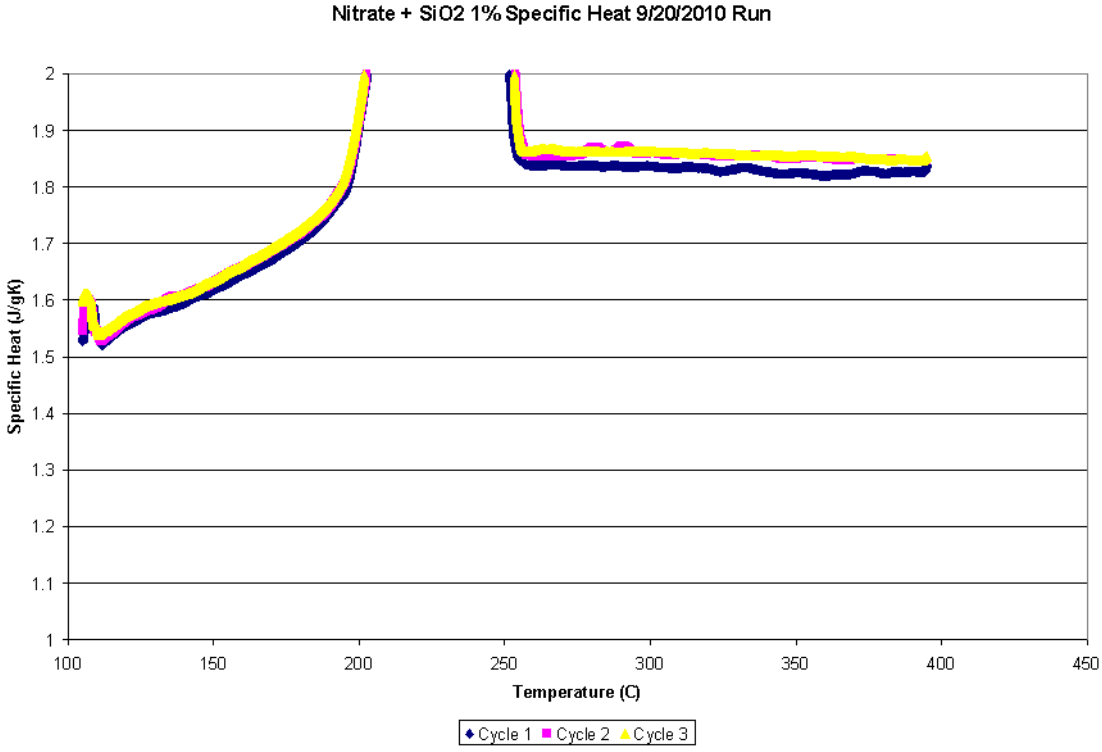
Nitrate + SiO2 1% Specific Heat 9/20/2010 Run
Specific Heat (J/gK)
2
1.9
1.8
1.7
1.6
1.5
1.4
1.3
1.2
1.1
1
100
150
200
250
300
350
400
450
Temperature (C)
Cycle 1
Cycle 2
Cycle 3

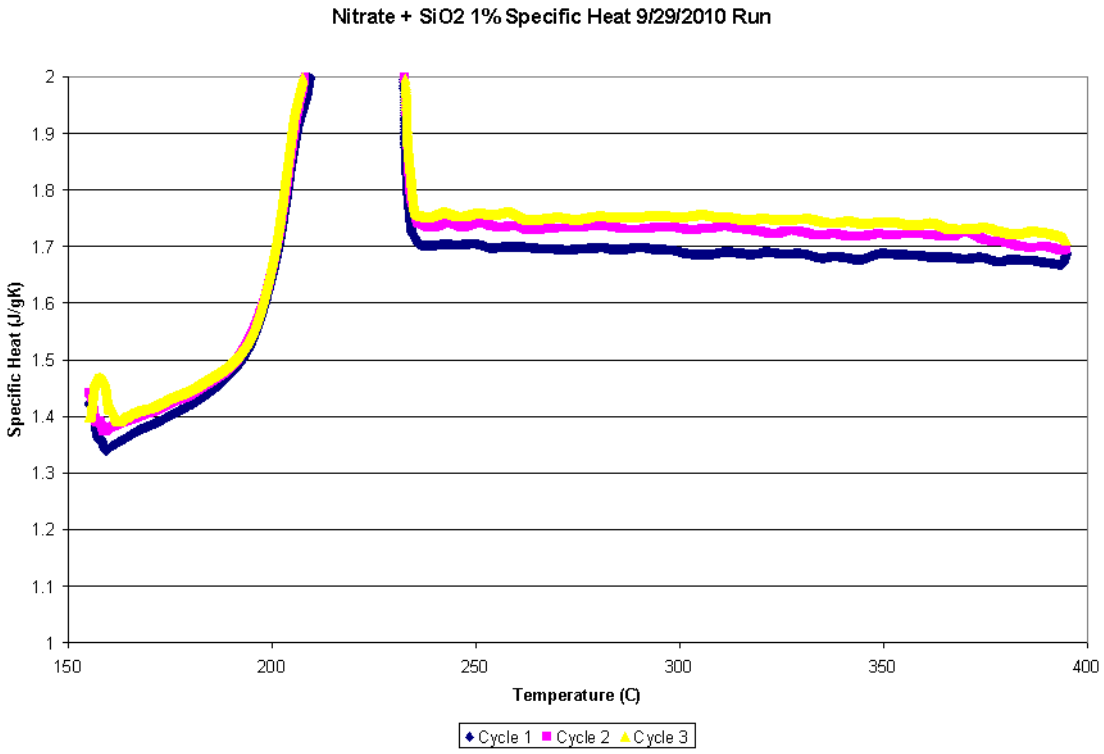
Nitrate + SiO2 1% Specific Heat 9/29/2010 Run
Specific Heat (J/gK)
2
1.9
1.8
1.7
1.6
1.5
1.4
1.3
1.2
1.1
1
150
200
250
300
350
400
Temperature (C)
Cycle 1
Cycle 2
Cycle 3

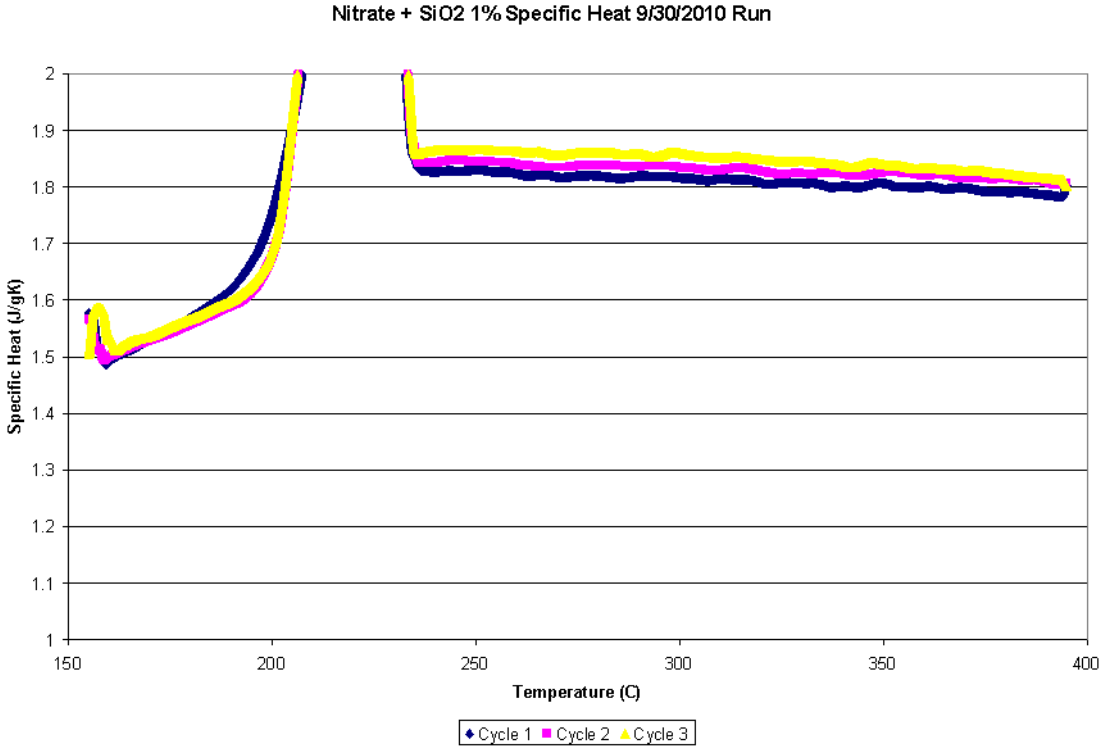
Nitrate + SiO2 1% Specific Heat 9/30/2010 Run
Specific Heat (J/gK)
2
1.9
1.8
1.7
1.6
1.5
1.4
1.3
1.2
1.1
1
150
200
250
300
350
400
Temperature (C)
Cycle 1
Cycle 2
Cycle 3

VITA

Name:	Matthew Robert Betts
Address:	Texas A&M University Department of Mechanical Engineering 3123 TAMU College Station, TX 77843-3123 c/o Thomas Lalk or Michael Schuller
Email Address:	gtg982h@tamu.edu
Education:	B.S. Mechanical Engineering, Georgia Institute of Technology, May 2007 M.S. Mechanical Engineering, Texas A&M University, May 2011